

Hubble Space Telescope Observations of Novae in M49

Laura Ferrarese, Patrick Côté and Andrés Jordán¹

Department of Physics and Astronomy, Rutgers University, New Brunswick, NJ 08854;
lff@physics.rutgers.edu; pcote@physics.rutgers.edu; andresj@physics.rutgers.edu

ABSTRACT

A search for novae in M49 (NGC 4472) has been undertaken with the *Hubble Space Telescope*. A 55-day observing campaign in F555W (19 epochs) and F814W (five epochs) has led to the discovery of nine novae. We find that M49 may be under-abundant in slow, faint novae relative to the Milky Way and M31. Instead, the decline rates of the M49 novae are remarkably similar to those of novae in the LMC. This fact argues against a simple classification of novae in “bulge” and “disk” sub-classes. We examine the Maximum-Magnitude versus Rate of Decline (MMRD) relation for novae in M49, finding only marginal agreement with the Galactic and M31 MMRD relations. A recalibration of the Buscombe–de Vaucouleurs relation gives an absolute magnitude 15 days past maximum of $M_{V,15} = -6.36 \pm 0.19$, which is substantially brighter than previous calibrations based on Galactic novae. Monte Carlo simulations yield a global nova rate for M49 of $\eta = 100^{+35}_{-30} \text{ year}^{-1}$ and a luminosity-specific nova rate in the range $\nu_K = 1.7 - 2.5 \text{ year}^{-1} 10^{-10} L_{K\odot}$. These rates are far lower than those predicted by current models of nova production in elliptical galaxies and may point to a relative scarcity of novae progenitors, or an increased recurrence timescale, in early-type environments.

Subject headings: galaxies: individual (M49, NGC 4472) — novae, cataclysmic variables — galaxies: star clusters — stars: distances

1. Introduction

As close binaries in which material is accreted onto the surface of a white dwarf, novae form the cataclysmic variable (cv) subclass of variable stars. With amplitudes of 10–20 magnitudes, they reach maximum magnitudes of $-6.5 \lesssim M_V \lesssim -10$ soon after the onset of

¹Claudio Anguita Fellow

thermonuclear runaway burning. These high luminosities — coupled with their occurrence in galaxies of all morphological types — suggests that novae have the potential to be useful distance indicators, provided that some aspect of their behavior near maximum light can be used as a standard candle.

While the earliest observations of extragalactic novae were reported by Ritchey (1917) and Shapley (1917), it was Hubble’s exhaustive study of M31 that probably constituted the first dedicated search for novae in an external galaxy (Hubble 1929). The full potential of novae as distance indicators became apparent following the discovery by Zwicky (1936) that their peak brightness correlates with their rate of decline, in the sense that bright novae fade more rapidly than their faint counterparts. Although the nature and calibration of this “Maximum Magnitude versus Rate of Decline” (MMRD) relation has been investigated on many subsequent occasions (*e.g.*, McLaughlin 1945; Arp 1956; Cohen 1985; Capaccioli et al. 1990; Livio 1992; Downes & Duerbeck 2000), these investigations have usually relied on observations for a handful of novae in the Galaxy or in M31, which, by virtue of its proximity and high luminosity, has remained the premier target for extragalactic novae surveys (*e.g.*, Arp 1956; Rosino 1973; Rosino et al 1989; Shafter & Irby 2001).

Despite some notable exceptions (*e.g.*, Graham 1979; Pritchett & van den Bergh 1985; 1987), studies of extragalactic novae have remained largely serendipitous in nature (*e.g.*, Ferrarese et al. 1996). While a few heroic attempts to detect and study novae in Virgo and Fornax ellipticals using ground-based telescopes (Pritchett & van den Bergh 1985; 1987; Shafter, Ciardullo & Pritchett 2000; Della Valle & Gilmozzi 2002) yielded light curves of varying quality for a few novae in a handful of galaxies, conclusions regarding the universality of the MMRD relation and its potential as a distance indicator rely almost entirely on observations of novae in the Galaxy, M31 and LMC (*e.g.*, Della Valle & Livio 1995). Accurate data for a sample of novae belonging to an elliptical galaxy with a well known distance would be invaluable in this regard, particularly since novae provide one of the few direct probes of compact binaries in such environments.

In this paper, we report the results of the first dedicated search for extragalactic novae with the *Hubble Space Telescope (HST)*. *HST* is an ideal instrument for such a survey thanks to its high spatial resolution, its ability to reach faint magnitudes in relatively short exposures, and the opportunity to schedule observations according to a pre-defined, optimized sequence. Our target, M49 (NGC 4472), is an obvious choice for several reasons. Not only it is the first ranked member of the Virgo Cluster, it is also the optically brightest galaxy in the local supercluster. Moreover, a variety of distance estimates are available for both Virgo, and for M49 itself. In fact, M49 offers the opportunity to compare, and perhaps even calibrate, the nova MMRD relation directly against other Population II distance indicators

such as surface brightness fluctuations and globular clusters.

2. Observing Strategy

The *HST* observations of M49 began on April 09, 2001 using the Wide Field and Planetary Camera 2 (WFPC2) on board the Hubble Space Telescope (*HST*). A total of 38 F555W (\sim Johnson *V*) images, divided among 19 epochs, were obtained within a 55 day period, with the sequence ending on June 03, 2001. For epochs 14 to 18 of the sequence, F814W (\sim Johnson *I*) images were taken immediately following the F555W observations. The relevant parameters of the observations are summarized in Table 1. All images were obtained at the same telescope roll angle. To facilitate removal of cosmic rays, exposures taken at each epoch shared the same pointing; however, the telescope was dithered by $0''.6$ between different epochs, to allow for accurate removal of CCD anomalies (e.g. hot or dead pixels). To maximize the number of novae outbursts, the center of M49 was placed close to the intersection of the four WFPC2 chips (Figure 1).

The temporal sequence and duration of the exposures were chosen with two main considerations in mind, namely: the need to produce well-sampled novae light curves (particularly near maximum light) and the need to follow their decline for at least two magnitudes thereafter. Because novae are not periodic (at least not on short timescales), there is always an obvious gain in lengthening the duration of monitoring programs. In practice, the length of our program was imposed by the pragmatic requirement of monitoring the field without a change in position angle, which *HST* can do for a maximum of about two months. This is longer than the decline rate for most novae (Capaccioli et al. 1989; Capaccioli et al. 1990; Downes & Duerbeck 2000), and therefore adequate for our purposes.

Prior to outburst, nova progenitors are obviously much too faint to be detected at the distance of M49. Following outburst, they reach maximum light rather quickly (typically within a few days) and then decline over much longer periods: from several days to a few months. A two day interval between visits was deemed sufficient to sample the light curve adequately both before and immediately after maximum. In the interest of keeping the total time request for the program within reasonable limits, M49 was originally scheduled to be monitored every two days with the F555W filter for the first 14 epochs (26 days), and every five days thereafter for the final five epochs (25 additional days) with both the F555W and F814W filters. Although novae outbursts occurring during the second half of the sequence might not be optimally sampled, it was hoped that the time and magnitude at maximum, as well as the rate of decline, could be recovered with the aid of the color information (Ferrarese et al. 1996; see also §4.1) and by employing the well-sampled light curves of novae discovered

during the first part of the program as templates.

The observing strategy discussed above was disturbed by a telescope safing event which occurred from 04/28/2001 to 04/30/2001. Because of this interruption, what was planned to be the eleventh epoch of our sequence was skipped and rescheduled at the end of the program, leaving an unfortunate four day gap during the finely sampled portion of the observing sequence.

3. Data Analysis

3.1. Data Reduction

The WFPC2 consists of four separate 800×800 CCD detectors: three Wide Field Camera (WFC) chips, with a pixel size of 0.10 arcsec and a field of view of 1.3×1.3 arcmin per chip, and one high resolution Planetary Camera (PC1), with a pixel size of 0.046 arcsec and a field of view of 36×36 arcsec. The gain and readout noise are about $7 \text{ e}^-/\text{DN}$ and 5 e^- respectively. Further details about the instrument can be found in the *HST* WFPC2 Instrument Handbook (Biretta et al. 2001). All of the M49 observations were obtained with the telescope guiding in fine lock, which achieves a nominal pointing stability of about 3 milliarcseconds.

The reduction of the M49 frames followed the standard pipeline maintained by the Space Telescope Science Institute (STScI), and included correction of small A/D errors; subtraction of a bias level for each chip; subtraction of a superbias frame; subtraction of a dark frame; correction for shutter shading effects and division by a flat field. For each filter, two back-to-back exposures were obtained to aid in the removal of cosmic rays. After standard reduction, but prior to performing the photometric analysis, these exposures were combined, and cosmic rays flagged and removed by comparing the difference in values between pairs of corresponding pixels to a local sigma calculated from the combined effects of Poisson statistics and local noise. The final, reduced, cosmic ray cleaned set of images consists of 19 F555W and five F814W frames. As a final step prior to photometric reduction, the vignetted edges of each chip were blocked and the geometric distortion of the WFPC2 optics was corrected using a pixel area map, following Stetson et al. (1998).

3.2. Photometric Analysis

Photometric analysis of the data was performed using a variant of DoPHOT (Schechter et al. 1993), developed specifically to handle the peculiarities of the *HST*/WFPC2 Point Spread Function (PSF) (Saha et al. 1994). As is standard procedure (e.g. Saha et al. 1996), DoPHOT was first run on deep F555W and F814W “template” frames made by coadding all 38 F555W and 10 F814W images, respectively. To prevent DoPHOT from triggering on an unreasonable number of noise spikes, a minimum $S/N = 4$ was required for object detection. The resulting master star list was then used as a position reference when DoPHOT was run on each individual frame. Using this approach, the completeness limit of the resulting photometry reaches fainter magnitudes than it would if DoPHOT were to be run directly on each individual epoch without the aid of a master star list. Furthermore, the results are more robust against residual cosmic rays which might affect individual frames.

The major challenge posed to the photometry comes from the fact that the vast majority of the point-like objects in the WFPC2 field are globular clusters belonging to M49’s rich system. At the distance of Virgo, globular clusters are marginally resolved, so that their PSF differs from the stellar PSF (and indeed varies with the size of the cluster). Because DoPHOT constructs its PSF directly from the brightest and most isolated objects in the image, in the case of M49 such a PSF might not adequately represent truly unresolved objects, such as novae. If this were the case, then the nova photometry could be compromised since the photometric corrections needed to convert the fitted DoPHOT magnitudes to conventional magnitudes (see below) would be appropriate for the globular clusters only.

Fortunately, this appears not to be the case. For a few of the epochs, the fitted DoPHOT magnitudes (which are simply related to the height of the fitted PSF) were compared to those measured from test runs in which DoPHOT was forced to use a fixed PSF, constructed from *HST*/WFPC2 observations of the globular clusters Pal 4 and NGC 2419 (Stetson et al. 1998). No significant offsets or scale errors were measured for either filter, indicating that the photometry is not affected by the small PSF broadening driven by the globular clusters.

DoPHOT fit magnitudes differ from ‘conventional’ magnitudes by an additive aperture correction, which can be calculated as the difference between fit magnitudes and aperture magnitudes, provided that the latter can be obtained for a sufficient number of bright, isolated stars in the field. Since such stars are not available for M49, a more robust approach is to use aperture corrections measured from unrelated F555W and F814W WFPC2 observations of a densely populated field in the Leo I dwarf galaxy (Saha et al. 1996). These images contain a multitude of stars across the entire field, allowing to quantify the positional dependence of the aperture corrections due to the spatial variations of the PSF. Conventionally, aperture magnitudes are measured within a $9'' \times 9''$ aperture; although it does not contain

the total light from a star, this aperture is large enough that PSF changes across the field, changes in focus over time, and small changes in jitter from one exposure to another do not affect the fraction of the total light that lies within this aperture. Finally, the $m_{9 \times 9}$ magnitudes obtained in this way were converted to the ‘ground system’ magnitudes F555W and F814W as defined in Holtzman et al. (1995) using the zero points derived from observations of ω Cen (Hill et al. 1998). In practice, this transformation is applied only to the results from the deep, template frames. Once the objects from the individual epochs are matched to their counterparts on the template, the offset for the individual epoch is evaluated from the ensemble average of magnitude differences (object by object) between that particular epoch and the template frame.

Following Holtzman et al. (1995), F555W and F814W magnitudes can be converted to V and I by applying a correction which depends on the color of the object under consideration. While color information is not always available for the novae, this correction is always smaller than 0.02 mag in V and 0.03 mag in I over the color interval $0.2 < (V - I) < 0.7$ mag, a range that is typical for novae (see, *e.g.*, van den Bergh & Younger 1987). Although systematic, this error is insignificant compared to the other sources of errors which enter our analysis, and will be neglected for the remainder of this paper.

3.3. Variable Star Search

Variability was searched for in the F555W frames using two independent methods. The first method applies a simple χ^2 test to the DoPHOT photometry for each object. The second method is similar to the image subtraction technique described by Alard & Lupton (1998), and makes no use at all of the DoPHOT photometry.

For any object detected by DoPHOT in at least two of the F555W frames, a reduced χ_r^2 was calculated as

$$\chi_r^2 = \frac{1}{(n-1)} \sum_i^n \frac{(m_i - \bar{m})^2}{\sigma_i^2}, \quad (1)$$

where m_i and σ_i are the magnitude and rms error of a particular object as measured in the i -th epoch, \bar{m} is the magnitude of the same object averaged over all epochs, and n is the number of epochs in which the object is detected. An object was flagged as variable if $\chi_r^2 \geq 3$; this is effectively equivalent to selecting objects whose magnitude fluctuates around the mean by 1.7σ on average.

Most of the objects flagged are, in fact, not intrinsically variable; rather, the large χ^2 is triggered by various anomalies in the images (e.g. residual cosmic ray events). A visual inspection of the light curve for each putative variable was sufficient to identify and reject these cases. The remaining candidates were visually inspected by blinking all of the individual frames against each other. The final list consists of nine bona-fide novae, all in the WFC chips (§4). Aperture photometry performed for each nova on all epochs in which the nova was detected provided an additional confirmation as to the reliability of the DoPHOT photometry.

The image subtraction technique can be considered as a “visual” application of the χ^2 method described above. First, all epochs are shifted to a common reference frame. A standard deviation frame is then created as:

$$stdev(x, y) = \sqrt{\frac{\sum_i [f_i(x, y) - \bar{f}(x, y)]^2}{18}}, \quad (2)$$

where $f_i(x, y)$ is the number of counts detected at pixel (x, y) in the i – *th* epoch F555W frame, and $\bar{f}(x, y)$ is the mean flux at the same pixel, averaged over all epochs. To avoid hot pixels and/or single cosmic ray hits that inflate the standard deviation, at each pixel, the epoch with the largest value of $f_i(x, y)$ is excluded from the summation in equation 2. All objects detected at the 2σ level relative to the mean local background in the standard deviation frame were then visually inspected by blinking all of the original frames against each other. This procedure recovered all of the nine novae flagged by the χ^2 test, but did not produce any additional detections.

The location of the nine novae found in M49 is shown superimposed to gray scale images of each chip in Figures 2-4, and on an isophotal contour of M49 in Figure 5. Zoomed-in snapshots of the novae around maximum light are shown in Figures 6 and 7. The coordinates of the novae are given in Table 2, while Table 3 lists the magnitudes at each epoch. Light curves are shown in Figures 8-10.

4. The Novae Light Curves

Can we be sure that the nine variable objects are indeed novae belonging to M49? We immediately rule out the possibility that they are Galactic RR Lyrae or Cepheid variables on the basis of their distinctive light curves: none of the light curves is periodic, the amplitude of variations would be atypically large for either class of variables, and the variation time scale is too long for RR-Lyrae variables. Furthermore, RR-Lyrae variables or Cepheids

reaching apparent magnitudes of $V \gtrsim 22$ would need to have distances $\gtrsim 250$ kpc, placing them outside the Galaxy. Nor could the variables be lower main sequence flare stars in the Galactic halo since variability in such stars occurs rapidly, on timescales of minutes to hours (Hoffmeister, Richter & Wenzel 1984). The possibility that the variables are distant AGNs is likewise untenable: optical fluctuations of 1–3 magnitudes in QSOs and Seyfert galaxies typically happen on timescales of several months to years, rather than weeks (Peterson 2001). Furthermore, there is no evidence for a nonstellar appearance in any of the sources.

Distant supernovae are also unlikely candidates. Over the redshift range $0.3 \lesssim z \lesssim 1.2$, Type Ia supernovae will have magnitudes of $20.5 \lesssim V \lesssim 26.5$ at peak brightness (*e.g.*, Schmidt et al. 1998; Nobili et al. 2003), falling by ~ 0.7 magnitudes about 15 days later (*e.g.*, Hamuy et al. 1996). Although such distant supernovae would resemble novae in M49, the number expected in our survey is far too low. The rate of faint, Type Ia supernovae (which, at these magnitudes, outnumber Type II supernovae by a wide margin) is $\sim 160 \text{ deg}^{-2} \text{ year}^{-1}$ over the range $0.3 \lesssim z \lesssim 1.2$ (Pain et al. 2002). Our WFPC2 field covers an area of 5.66 square arcminutes and the survey duration is 55 days, giving a dismal ~ 0.04 distant supernovae expected in our survey.

More likely, the variables belong to M49 itself, as indicated by the fact that their spatial distribution (Figures 2-5) is not uniform across the field, but concentrates towards the center of the galaxy. Based on the light curves, variation amplitudes, and the fact that M49 is an E2 galaxy, we can again eliminate the possibility of long period variables or Cepheids. Microlensing events of the sort described by Baltz & Silk (2000; 2001) are also unlikely. Scaling from the event rate observed in M87, we expect approximately one event per month for M49 (E. Baltz; private communication) with no stipulation on timescale. From Figure 2 of Baltz & Silk (2000), we expect events of duration $t_{\text{FWHM}} \gtrsim 5$ days to comprise only a small fraction of the overall event rate. Moreover, microlensing light curves are expected to be symmetric around the peak time, which is not the case for any of the five objects for which our observations bracket the inferred maximum. We conclude that microlensing is not a significant source of contamination, leaving novae in M49 as the only realistic explanation for the observed flares.

Figure 11 shows a comparison between the cumulative distribution for the novae and the underlying galaxy light, measured in the V -band. As is apparent from Figures 2-5, the novae appear to be more centrally concentrated than the galaxy light: a KS test shows an 8% probability that they were drawn from the same distribution. Artificial star tests (§7) predict that only novae in the innermost ~ 5 arcsec of the galaxy will elude detection, and that beyond 17 arcsec even novae which have already declined by two magnitude at the time of discovery will be recovered. Missing novae in the innermost region would of course

only exacerbate the contrast between the novae distribution and the underlying galaxy light. Pritchett & van den Bergh (1987) also found that the cumulative distribution of novae in M49 does not follow the underlying galaxy light, although in their case the novae seem to be under-represented in the outer ($r > 40''$) parts of the galaxy. These somewhat puzzling results deserve further investigation in future surveys.

4.1. Determination of Light Curve Parameters

As will be discussed in detail in §6, the use of novae as distance indicators requires an accurate knowledge of their light curves, in particular, the maximum magnitude, V_{\max} , the time of maximum light, t_{\max} , and the time taken to decline two magnitudes from peak brightness, t_2 . Here we discuss the determination of these parameters for our sample of novae.

Novae #1,2,3,8: Unfortunately, the light curves for all of these novae were already declining from maximum brightness at the outset of our program, making direct measurements of V_{\max} and t_{\max} impossible. Instead, we take $V_{\max} \leq V(1)$ and $t_{\max} \leq t(1)$, where $V(1)$ and $t(1)$ refer to the magnitude and time of the first epoch. The time taken for the novae to decline in brightness by two magnitudes, t_2 , and the corresponding decline rates, $\nu_d \equiv 2/t_2$ can be bracketed more securely, since the observed light curves are very nearly linear for the first few epochs. Both are therefore estimated directly from weighted least-squares fits to the V -band light curves using epochs 1–5 (nova #1), 1–6 (nova #2), 1–3 (nova #3), and 1–10 (nova #8).

Nova #4: The nova is detected both before and after maximum. Although the entire light curve is only sampled at 5-day intervals, both V and I data are available post-maximum, allowing a precise determination of t_{\max} . According to van den Bergh & Younger (1987), novae at maximum light have $(B - V)_0 = 0.23 \pm 0.06$, corresponding to a spectral type between A7 and F0. From Zombeck (1990), this translates to $(V - I)_0 = 0.37 \pm 0.10$, or $(V - I)_{\max} = 0.40 \pm 0.10$ in the case of M49, adopting a total (foreground plus internal) reddening to the galaxy $A(V) = 0.07$ and the relative extinction coefficients from Schlegel, Finkbeiner & Davis (1998). Linear extrapolations from $V(14)$, $V(15)$, $I(14)$ and $I(15)$ then give $t_{\max} = 2452039.04 \pm 1.11$. The implied magnitudes at this time are $V_{\max} = 23.33 \pm 0.13$ and $I_{\max} = 22.93 \pm 0.03$, where the main contribution to the error comes from the uncertainty in the intrinsic color at maximum. This nova has not yet faded by two magnitudes by the end of our observing sequence, but a weighted linear least-squares fit to $V(14)$ – $V(19)$ — further constrained to pass through V_{\max} — gives $t_2 = 52.00 \pm 4.21$ days.

Nova #5: As in the preceding case, the nova is detected during its rise to maximum, and V and I light curves are available during its post-maximum evolution. Extrapolating to $(V - I)_{\max} = 0.40 \pm 0.10$ on the basis of $V(15)$, $V(16)$, $I(15)$ and $I(16)$ gives $t_{\max} = 2452041.42 \pm 1.95$, $V_{\max} = 23.10 \pm 0.52$ and $I_{\max} = 22.70 \pm 0.42$. A least-squares fit to V_{\max} , $V(14)$ and $V(15)$ yields $t_2 = 7.53 \pm 1.14$ days.

Nova #6: Although this nova is observed during its rise to maximum, only limited color information is available during its post-maximum evolution. We assume that peak brightness occurred midway between epochs 8 and 9, so that $t_{\max} = 2452023.46 \pm 0.50$. Extrapolations based on $V(9)$, $V(10)$ and $V(11)$ then yield $V_{\max} = 23.33 \pm 0.28$. A weighted least-squares fit to $V(9)$ – $V(15)$ gives $t_2 = 19.30 \pm 0.86$ days.

Nova #7: Two observations of this nova are available prior to maximum light: $V(9)$ and $V(10)$. In an unfortunate example of Murphy’s law, the period around maximum coincided with the telescope safing event discussed in §2 (the light curve of nova 9 also suffered from the safing). Extrapolating forward from $V(9)$ and $V(10)$, and backwards from $V(11)$ and $V(12)$, gives $t_{\max} = 2452027.33 \pm 0.50$ and $V_{\max} = 22.72 \pm 0.36$. Based on this V_{\max} , and interpolating between $V(13)$ and $V(14)$, we find $t_2 = 11.68 \pm 0.83$ days.

Nova #9: In this case, there is some ambiguity concerning the precise time of maximum. Given the short rise time for most novae, we think it most likely that maximum brightness occurred shortly after epoch 11. The other possibility — that maximum brightness occurred before epoch 11 and after epoch 10, when the nova was not detected — cannot be excluded given the fact that novae light curves do not always exhibit a monotonic decline after maximum (see, *e.g.*, nova #6). Working under the assumption that peak brightness occurred midway between epochs 11 and 12, at $t_{\max} = 2452031.45 \pm 0.50$, extrapolating from $V(12)$ and $V(13)$ gives $V_{\max} = 23.74 \pm 0.22$. This nova never fades by two magnitudes from V_{\max} so we take $t_2 = 37.16 \pm 2.86$ days based on a linear least-squares fit to $V(12)$ – $V(19)$, constrained to pass through V_{\max} .

Light curve parameters for all nine novae are summarized in Table 6. From left to right, the columns of this table record the identification number, the time of maximum light, the V -magnitude at maximum, the absolute V magnitude for $(m - M) = 31.06 \pm 0.06$ and $A(V)_g = 0.07$ (see §6.1), the time taken for the light curve to decline by two magnitudes, and the corresponding decline rate.

5. The Distribution of Novae Decline Rates

It has been suggested on a number of occasions (*e.g.*, Duerbeck 1990; Della Valle & Duerbeck 1993; Della Valle 2002) that there exist two populations of novae: bright, rapidly declining “disk” novae and faint, slowly declining “bulge” novae. Since M49 is an elliptical galaxy consisting mainly of old and intermediate-age stars (*e.g.*, Trager et al. 2000; Cohen et al. 2003), one would expect our sample of novae to consist entirely of faint objects with long decline times. The cumulative fraction of novae as a function of decline rate, $\nu_d = 2/t_2$ is shown in Figure 12, compared to the cumulative rates (again measured as $\nu_d = 2/t_2$) observed for M31 (Capaccioli et al. 1989), the LMC (Capaccioli et al. 1990) and the Milky Way (Downes & Duerbeck 2000). The M49 sample seems to behave exactly the opposite as expected: *i.e.*, faint objects with long decline rates are under-abundant. This is unlikely due to an observational bias since our photometry is essentially complete down to $V = 25.5$ mag. Even the faintest novae are expected to reach $23.8 \lesssim V \lesssim 24.5$ mag at maximum (see §6.2) and decline by one magnitude or more during the length of our observing period: if present, they should have been detected. A Kolmogorov-Smirnov test yields significance levels of 21% and 49% for the null hypothesis that the M49 novae sample and those of the Milky Way and M31, respectively, are drawn from the same population. However, the corresponding significance level for the M49 and LMC samples is 99%.

It is worth noting that some of the decline rates for LMC and Milky Way novae, and most of those for novae in M31, are based on photographic magnitudes. Since novae decline more slowly in B than V , the decline rates for the LMC, Milky Way and M31 novae should be increased somewhat relative to those in M49, which are measured in the V band. According to Van den Bergh and Younger (1987), $\log t_2(V) = 0.953(\pm 0.013) \log t_2(B)$. Correcting the Milky Way and LMC samples produces no difference as far as the KS test is concerned. For the M31 sample, it is not always clear which novae have photographic magnitudes and which have V – band magnitudes. In the extreme case in which the decline rates for all novae are corrected, the disagreement between the M49 and M31 samples becomes less severe, but a KS test still returns a significance level of only 84% that the two samples are drawn from the same population.

The LMC novae are usually regarded as prototypical examples of young, disk novae. We conclude that our survey provides no clear support for a simple classification of novae into a disk and bulge populations, although a larger sample of novae in additional early type galaxies is needed for a clear resolution of the issue.

6. Novae as Distance Indicators

The main goal of our program is to assess the usefulness of novae as standard candles and, if possible, to provide a calibration of the various relations which could establish novae as reliable distance indicators (*e.g.*, Livio 1992). Because such relations are, at present, calibrated exclusively with novae in two spiral galaxies (*i.e.*, M31 and the Galaxy), their applicability to early type galaxies remains untested. M49 was chosen for this program not only because of its brightness, but also because of the availability of secure distance estimates. Here, we focus on two Population II distance indicators — surface brightness fluctuations (SBF) and the globular clusters luminosity function (GCLF).

6.1. Distance Calibration via SBF and Globular Clusters

Tonry et al. (2001) report an SBF distance modulus of $(m - M)_0 = 31.06 \pm 0.10$ for M49². Since the best available Maximum Magnitude versus Rate of Decline (MMRD) relation for novae is based almost entirely on observations of M31, it is also of interest to know the distance to M31 on the same SBF scale, to facilitate the comparison of novae in the two galaxies. According to Tonry et al. (2001), the SBF distance of M31 is $(m - M)_0 = 24.40 \pm 0.08$, giving a difference in distance moduli between the two galaxies of $\Delta(m - M)_0 = 6.66 \pm 0.13$ mag.

The GCLF has been claimed to be a first class distance indicator (*e.g.*, Jacoby et al. 1992) although concerns have also been raised (Ferrarese et al. 2000). Our co-added images of M49 are the deepest ever obtained for this galaxy; outside of the central $20''$, our deep images reach $V \simeq 25$ with better than 90% completeness. The GCLF, $\phi(V)$, can therefore be derived directly from our data, providing an independent check of the adopted SBF distance.

To do so, the co-added, cosmic ray cleaned, deep F555W and F814W images (§3.1) were background-subtracted via multi-resolution wavelet filtering using the MR/1 package (Starck, Bijaoui & Murtagh 1998). Object detection and photometry on the background subtracted frames was performed with SExtractor (Bertin & Arnouts 1996), using a detection threshold of three connected pixels above 3.5σ . Object catalogs for the separate F555W and F814W frames were then matched with a matching radius of two pixels, and calibrated

²The SBF calibration adopted by Tonry et al. is based on Cepheid distances to nearby galaxies which use the same *HST*/WFPC2 photometric calibration adopted for the novae in this paper. Although the photometric scale of the WFPC2 has since been refined (Stetson 1998), the novae photometry and SBF distance are mutually consistent.

V and I magnitudes were obtained following Holtzman et al (1995, see also §3.2). The matched catalog was then trimmed to exclude objects with $V < 25$ or colors outside the range $0.7 \leq (V - I) \leq 1.45$.

Our final catalog consists of 389 globular cluster candidates. For comparison, Larsen et al. (2001) have recently carried out a study of the M49 globular cluster system based on three partially overlapping fields. Using the same magnitude and color selection criteria as described above, we find their catalog to contain a total of 661 objects; the larger sample is a consequence of the greater areal coverage of their survey. A comparison of the M49 GCLFs derived in this paper and Larsen et al. (2001) is given in Figure 13 (note that our luminosity function has been scaled upwards by the ratio of the sample sizes, $661/389 \approx 1.7$). There is good agreement between the two luminosity functions. Following the usual procedure of parameterizing $\phi(V)$ as a Gaussian, we find best-fit values for the turnover and dispersion to be $V^{\text{TO}} = 23.87 \pm 0.06$ and $\sigma = 1.43 \pm 0.09$. With the calibration of Harris (2001), this turnover corresponds to a distance modulus of $(m - M) = 31.13 \pm 0.09$. This best-fit Gaussian is shown by the solid curve in Figure 13. If we instead choose to fix the location of the turnover based upon the SBF distance modulus of Tonry et al. (2001) and the M_V^{TO} calibration of Harris (2001), we find $V^{\text{TO}} \equiv 23.80$ and $\sigma = 1.42 \pm 0.07$. The corresponding luminosity function is shown as the dashed curve in Figure 13. We conclude that the SBF and globular cluster luminosity function methods yield highly consistent results for the distance of M49.

In what follows, we adopt the SBF M49 distance modulus of $(m - M) = 31.06 \pm 0.10$ mag, corresponding to a distance of 16.3 ± 0.7 Mpc.

6.2. The Maximum Magnitude versus Rate of Decline Relation

Although a relation between the magnitude reached by novae at maximum and their rate of decline was first proposed in 1936 by Zwicky, a theoretical and phenomenological description of this MMRD relation has proven remarkably elusive. From an observational standpoint, the main obstacle remains the small number of galaxies for which large samples of novae with high-quality light curves have been collected. The list includes only three objects: M31, with ≈ 55 novae (Capaccioli et al. 1989), the Galaxy, with a few dozen objects (Downes & Duerbeck 2000), and the LMC, with about 10 novae (Capaccioli et al. 1990). In many cases, analysis of the light curves is further complicated by the fact that observations are available in non-standard, photographic bandpasses.

These concerns notwithstanding, it is known that the Galactic MMRD relation can be

fit reasonably well with a power law (Cohen 1985). Based on new distances derived from expansion parallaxes for a sample of Galactic novae, Downes & Duerbeck (2000) find:

$$M_{V,max} = (-11.32 \pm 0.44) + (2.55 \pm 0.32)\log(t_2) \quad (3)$$

where t_2 is the time it takes for the nova to decline by two magnitudes from peak brightness, $M_{V,max}$. Both the M31 sample, and the combined M31 and LMC samples, are better described in terms of a “stretched” S-shaped curve, whose most recent calibration is given as (Della Valle & Livio 1995):

$$M_{V,max} = -7.92 - 0.81\arctan\frac{1.32 - \log t_2}{0.23} \quad (4)$$

Fitting a similar function to the sample of Galactic novae produces a zero point consistent with the one found for M31, but a significantly higher contrast between faint and bright novae (Downes & Duerbeck 2000), although it should be pointed out that the quality of the fit is not significantly improved over that provided by the single power law given in equation 3:

$$M_{V,max} = -8.02 - 1.23\arctan\frac{1.32 - \log t_2}{0.23}, \quad (5)$$

It is important to note that there is no theoretical explanation for a relation of the kind shown in equations 4 and 5. In fact, Downes & Duerbeck (2000) argue that a better, and physically motivated, characterization of the Galactic MMRD relation might be expressed in terms of a broken power-law, in which novae are divided in two distinct subgroups on the basis of the shape of the light curve and the detailed physics of the outburst (Duerbeck 1981).

Figures 14 and 15 compare the location of the nine M49 novae in the MMRD plane (circled points) with those of M31 and the Milky Way, respectively. Absolute, dereddened magnitudes and decline rates for the Milky Way novae are listed by Downes & Duerbeck (2000, Table 5), and can be easily scaled for comparison with the M49 sample by adopting $(m - M)_0 = 31.06 \pm 0.10$ mag and $A(V)_g = 0.07$ for M49 (from Tonry et al. 2001, using the relative extinction coefficients of Schlegel, Finkbeiner & Davis 1998). Decline rates and apparent, reddened, photographic maximum magnitudes for the M31 novae are from Table IV of Capaccioli et al. (1989). The photographic magnitudes can be transformed to the V -band according to the relation $V \approx m_{pg} - 0.06$, but scaling the M31 novae samples to the distance and reddening of M49 proves to be a non-trivial task. Although the distance

to M31 is well known (e.g. Ferrarese et al. 2000, we adopt here $(m - M)_0 = 24.40 \pm 0.08$ mag from Tonry et al. 2001), the total extinction to the galaxy is not. The RC3 reports values of $A(B)_i = 0.67$ mag for the B -band extinction internal to M31, based on the galaxy inclination and Hubble type. The foreground (Galactic) reddening is generally taken as $E(B - V) = 0.08$ mag, corresponding to $A(B) = 0.35$ mag (see Bianchi et al. 1996 for a comprehensive discussion). Given these estimates, the total V -band extinction to M31 is therefore $A(V) \sim 0.77$ mag, where we have adopted $A(B)/A(V) = 1.321$ following Schlegel, Finkbeiner & Davis (1998). This value can be compared to the one derived by Bianchi et al. (1996) using *HST* UV observations of eight blue supergiants. Their study points to a total reddening to M31 in the range $E(B - V) = 0.13 - 0.20$ mag, which translates to a V -band total extinction in the range $A(V) = 0.43 - 0.66$. For consistency with the absorption adopted for other galaxies with measured novae rates (to be discussed in §7), in what follows we adopt $A(V) \sim 0.77$ mag for M31, with a 20% uncertainty.

Filled and open squares in Figure 14 represent novae judged by Capaccioli et al. to have light curves of good and fair quality, respectively. Absolute magnitudes are shown on the right vertical axis. The dashed curves in Figures 14 and 15 represent the best fit to the M31 sample (from Capaccioli et al. 1989), and the MW sample (Downed & Duerbeck, 2000; equation 5) respectively. Residuals between these relations and the M49 novae are shown in the lower panels. The solid line in Figures 15 is the best power law fit to the Galactic sample (equation 3).

The M49 sample is formally consistent with the Milky Way sample, while the agreement with the M31 data is less secure. Restricting ourselves to the five M49 novae with measured V_{\max} and ν_d , the mean offsets between M49 and the best fitting relations to the M31 and Milky Way samples shown by the dashed lines in Figures 14 and 15 are -0.50 ± 0.15 (random) ± 0.20 (systematic) mag and -0.18 ± 0.15 (random) ± 0.10 (systematic) mag respectively. In the above estimate, the systematic error arises from the uncertainties in the distances and reddenings to M31 and M49, while the random component arises from the uncertainties in the magnitudes at maximum for the M49 novae. Although the M49 and M31 samples disagree at the 2σ level, larger uncertainties in the internal extinction to the galaxy than considered here are possible. The root-mean square scatters of the M49 relation around the M31 and MW MMRD relations are 0.74 mag and 0.85 mag respectively; in both cases, there appears to be a systematic trend for fast novae to be under-luminous, and slow novae to be over-luminous compared to expectations, although the small number of objects does not allow us to speculate any further.

A formal fit to the M49 sample, using the same relations given in equations 4 and 5, allowing only the zero point to vary, and accounting for errors in the magnitudes, produces:

$$M_{V,max} = (-8.27 \pm 0.59) - 0.81 \arctan \frac{1.32 - \log t_2}{0.23}; \text{ rms} = 0.82 \text{ mag} \quad (6)$$

and

$$M_{V,max} = (-8.56 \pm 0.86) - 1.23 \arctan \frac{1.32 - \log t_2}{0.23}; \text{ rms} = 1.24 \text{ mag} \quad (7)$$

respectively. The large scatter about these relations suggests that, regardless of the details of the calibration, caution is needed when deriving distances via the MMRD relation.

6.3. The Buscombe and de Vaucouleurs Relation

Buscombe & de Vaucouleurs (1955) first noted that the absolute magnitude 15 days after maximum light, M_{15} , appears to be roughly the same for all novae. The existence of a time, or time interval, after maximum at which the absolute brightness of novae are approximatively constant follows from the MMRD relation (*e.g.*, Shara 1981b) — because brighter novae decline faster than fainter ones, the light curves must intersect sometime after maximum. The calibration of M_{15} as a standard candle has been attempted on many occasions (*e.g.*, Shara 1981a; van den Bergh & Younger 1987; Cohen 1985; Downes & Duerbeck 2000), yielding a rather wide range in results.

Figure 16 shows light curves for the five novae in our sample (# 4, 5, 6, 7 and 9) for which both V_{\max} and t_{\max} can be measured directly from their light curves (see §4.1). Each light curve has been shifted in time so that maximum light occurs at $t \equiv 0$. Averaging the apparent magnitude at $t = 15$ days gives $V_{15} = 24.77 \pm 0.19$, corresponding to

$$M_{V,15} = -6.36 \pm 0.19 \text{ (random)} \pm 0.10 \text{ (systematic)} \quad (8)$$

where the random uncertainty represent the error in the mean, and the systematic uncertainty reflects the assumed errors on M49’s distance and extinction. The standard deviation about this mean value is $\sigma = 0.43$.

This determination of $M_{V,15}$ is strongly at odds with the value $M_{V,15} = -5.23 \pm 0.16$ found by van den Bergh & Younger (1987) from a sample of six Galactic novae with known expansion parallaxes. It is barely consistent with the value of $M_{V,15} = -5.60 \pm 0.45$ found by Cohen (1985) from her study of 11 novae with spatially resolved expansion shells, but it is in reasonable agreement with the value of $M_{V,15} = -6.05 \pm 0.44$ found by Downes & Duerbeck (2000) using the same method, but for a larger number of Galactic novae.

The lower panel of Figure 16 shows the mean novae magnitudes and standard deviations as a function of time after maximum. It is interesting to note that a rather small standard deviation ($\sigma = 0.37$ mag) is found at maximum. The mean magnitude at maximum for the five observed novae is $M_{V,max} = -7.89 \pm 0.17$ (random) ± 0.10 (systematic), although we strongly caution against using this estimate as a distance indicator. For instance, nova #2 was ≈ 0.6 magnitudes brighter than this at the onset of our program, at which time it was already declining from maximum.

Is it reasonable to use $M_{V,15}$ as a distance indicator? We can test this hypothesis on novae #1, 2, 3 and 8, which were already declining at the beginning of our program. If we assume that these novae reach $V = 24.77 \pm 0.19$ fifteen days after maximum, then using the available datapoints (Table 3), we can linearly extrapolate the light curve and infer $M_{V,max}$ and t_{max} . The V magnitudes at maximum found in this way are 20.87 ± 0.46 for nova # 1, 21.53 ± 0.20 for nova # 2, 17.86 ± 1.1 for nova # 3, and 23.08 ± 0.19 for nova # 4³. If these data are added to the maximum magnitude and rate of decline of the five novae for which both parameters are measured directly, and the MMRD relation given in equation (5) is fit to the data, a distance modulus to M49 of $(m - M)_0 = 30.67 \pm 0.71$ is obtained (the error accounts only for the uncertainties in the M49 data, not in the MMRD calibration). This is certainly consistent with Tonry et al. $(m - M)_0 = 31.06 \pm 0.10$, but hardly useful.

We conclude that the large standard deviation shown for $M_{V,15}$, coupled with the rather poor agreement between the different calibrations of $M_{V,15}$ based on samples of Galactic novae, suggest that one should exercise considerable caution when estimating distances with this method. This perhaps should come as no surprise since, as noted by Jacoby et al. (1992), several “exceptional” novae in M31 (*e.g.*, Arp 1, 2 and 3) offered clear counterexamples to the universality of the Buscombe & de Vaucouleurs relation.

7. Nova Rates

The nova rate is a fundamental property of any stellar population and represents a direct probe of the abundance of compact, mass-transfer binaries in the host galaxy. There have been some recent claims that the luminosity-specific nova rate varies along the Hubble sequence, with late-type galaxies being more efficient producers of novae than their early-type counterparts (*e.g.*, Della Valle et al. 1994; Yungelson, Livio & Tutukov 1997; Della Valle 2002; *c.f.* Shafter et al. 2000). M49, as an E2 galaxy and the optically brightest member of the local supercluster, presents an opportunity to measure the nova rate in an

³For this nova, the outburst is predicted to have occurred 1.8 ± 2.7 days after the first epoch.

extreme environment.

We use a Monte Carlo approach to measure the global nova rate in M49. The difference in distance moduli between M31 and M49 is taken to be $\Delta(m - M) = 6.66$, as discussed in §6.1. For an assumed global nova rate, η , we randomly select novae having maximum magnitudes and rates of decline given by the M31 relation of Capaccioli et al. (1989), displaced to the distance of M49. Light curves are then simulated by calculating V -band apparent magnitudes at the dates of the actual observations, assuming a linear decline from maximum light.

For each simulated nova, we randomly assign a galactocentric position assuming that the local nova rate correlates linearly with stellar mass density, and adopting the M49 surface brightness model presented in Côté et al. (2003). Any novae falling outside the regions of our survey are discarded. Artificial star experiments were carried out to determine the level of photometric completeness as a function of radius and magnitude. The results of these experiments were used to determine, on a case-by-case basis, if the simulated nova would be detected in our survey at the assigned radius and given its instantaneous magnitude at each epoch. We consider a simulated nova to be “discovered” if it is detected at two or more epochs and shows a variation in brightness that is larger than that expected on the basis of its photometric errors. We carry out 1000 simulations at each η , recording the number of times the number of detected novae in the simulations matched the observed number of novae. This process is repeated for global nova rates varying between $\eta = 0$ and 300 year^{-1} in steps of five.

The results of this exercise are plotted in Figure 17. The histogram shows the number of matches found in the Monte Carlo simulations, plotted against global nova rate. The vertical lines outline the best estimate of the global nova rate, $\eta = 100_{-30}^{+35} \text{ year}^{-1}$, where the quoted uncertainties refer to 68% confidence limits determined directly from the simulations.

How does this nova rate compare to those found in the literature? In a ~ 30 day campaign, Pritchett & van den Bergh (1987) visually identified eight novae in M49. Not accounting for incompleteness or detection biases, this yields a nova rate of $\eta = 160 \pm 57 \text{ year}^{-1}$ (for $(m - M)_0 = 31.0$), consistent with the value derived in this paper. The only other (undisturbed) giant elliptical galaxy for which a detailed search for novae has been undertaken is M87, the second brightest member of the Virgo cluster. On the basis of multi-epoch, ground-based $H\alpha$ imaging, Shafter et al. (2000) measured a global nova rate of $\eta = 91 \pm 34 \text{ year}^{-1}$ for this galaxy. Scaling our nova rate for M49 downwards by the ratio of the K -band luminosities of M49 and M87, we predict $\eta \simeq 70 \pm 23 \text{ year}^{-1}$ for M87, fully consistent with the nova rate of Shafter et al. (2000). On the other hand, our predicted nova rate for M87 is strongly at odds with the extreme rate of “200 to 300” year^{-1} found

for M87 by Shara & Zurek (2002)⁴. For instance, if we turn the argument around and scale the Shara & Zurek (2002) nova rate for M87 to the luminosity of M49, we would expect $280 \lesssim \eta \lesssim 425 \text{ year}^{-1}$. Our Monte Carlo simulations reveal that such high nova rates can be ruled out at better than 99.9% confidence.

The complete sample of galaxies having measured nova rates encompasses objects with widely different morphological types, luminosities and star formation histories. Relevant information for these galaxies is summarized in Table 7. Columns (1-3) give the galaxy name, morphological type from the NASA Extragalactic Database (NED) and global nova rate. Sources for these nova rates are given in the footnotes to the table. Note that there is some disagreement over the global nova rate in M33: Della Valle et al. (1994) quote a value of $\eta = 4.6 \pm 0.9 \text{ year}^{-1}$, while Sharov (1993) argues for an *upper limit* of $\eta \simeq 0.45 \text{ year}^{-1}$.

We follow the usual approach of normalizing the global nova rates by K -band luminosity (which more closely traces the mass in evolved stars). We consider two estimates for the total, dereddened K -band magnitudes $M_{K,0}$. A recent 2MASS release (Jarrett et al. 2003) lists total (extrapolated), reddened, K -band magnitudes for all galaxies (Column 5 of Table 7), with the exception of the LMC and SMC. We corrected the 2MASS magnitudes for both internal and Galactic extinction, using the B -band absorption $A(B)_i$ and $A(B)_g$ from the RC3 and Schlegel, Finkbeiner & Davis (1998) respectively (columns 7 and 8 of Table 7), and $A(K)/A(B) = 0.085$ (Schlegel, Finkbeiner & Davis 1998). $M_{K,0}$ can also be calculated by correcting the total B -band magnitude (from the RC3, column 4 of Table 7) for extinction, and then applying a mean, dereddened $(B - K)_0$ color (column 6 of Table 7, with references given in the footnotes). To transform the dereddened $M_{K,0}$ to a luminosity in solar units, we adopt the distance moduli given in column (9), and $M_{K,\odot} = 3.33 \text{ mag}$ (Cox 2000). Columns (10-11) give the luminosity-specific nova rates, ν_K , in the two cases in which the galaxy K -band luminosity is calculated starting from the RC3 B -band magnitudes, or adopted from the 2MASS analysis, respectively.

Before proceeding with an analysis of the behavior of ν_K among the full sample of galaxies, we pause to consider the implications of our measured nova rate for M49. Our best estimate of the luminosity-specific nova rate in M49, $\nu_K = 1.71 \pm 0.61 \text{ year}^{-1} 10^{-10} L_{K\odot}$ ($\nu_K = 2.52 \pm 0.91 \text{ year}^{-1} 10^{-10} L_{K\odot}$ when using the 2MASS data), is far smaller than predicted by theoretical models of nova production. For instance, Matteucci et al. (2003) have computed galactic nova rates as a function of mass and star formation history. Using the elliptical galaxy template models, and adopting a luminous mass of $\mathcal{M} \simeq 8 \times 10^{11} \mathcal{M}_\odot$ for M49 (Côté et al. 2003), we find the Matteucci et al. (2003) models to predict global nova rates in

⁴As cited in Matteucci et al. (2003).

the range $780 \lesssim \eta \lesssim 900 \text{ year}^{-1}$, nearly an order of magnitude larger than the observed value of $\eta = 100_{-30}^{+35} \text{ year}^{-1}$. Given the size of the discrepancy — and since the theoretical models were calibrated to reproduce the global nova rate of $\eta \simeq 25 \text{ year}^{-1}$ for the Milky Way — reconciling the models and observations for M49 may require global differences in the properties of the novae progenitors in the two galaxies. Obvious candidates would include a reduced binary fraction in M49 relative to the Milky Way, or longer recurrence timescales between outbursts.

Figure 18 shows ν_K plotted as a function of K -band luminosity for M49 (circled point) and each of the galaxies in Table 7 (dots). Note that M33 is plotted for both the high nova rate of Della Valle et al. (1994) and the upper limit of Sharov (1993). Excluding this galaxy, the weighted mean nova rate is $\langle \nu_K \rangle = 1.58 \pm 0.16 \text{ year}^{-1} 10^{-10} L_{K\odot}$ when $M_{K,0}$ is derived from the RC3 B -band magnitudes, and $\langle \nu_K \rangle = 2.41 \pm 0.27 \text{ year}^{-1} 10^{-10} L_{K\odot}$ when the 2MASS data are used.⁵

The $\sim 35\%$ increase in the luminosity-specific nova rates when the 2MASS data are used is a consequence of the 0.2 mag systematic difference between the two estimates of $M_{K,0}$, with the 2MASS magnitudes being fainter. It is unclear which estimate of $M_{K,0}$ is more reliable: compared to the 2MASS values, the RC3 B -band magnitudes are more robust against small errors in the sky estimates, but are very sensitive to extinction corrections, which can be very uncertain in the case of spiral galaxies. In either case, the luminosity specific nova rate in M49 appears to be in good agreement with the mean determined from the complete sample. Indeed, with the possible exception of the LMC, every galaxy for which a reliable measurement of ν_K exists appears to be consistent with a “universal” value of $\langle \nu_K \rangle \approx 1.6 - 2.4 \text{ year}^{-1} 10^{-10} L_{K\odot}$. These findings are fully consistent with those of Shafter et al. (2000).

This constancy of ν_K has implications for theoretical models of the galactic nova rates, and for possible dependences on morphological type and star formation history. Calculations by Yungelson, Livio & Tutukov (1997) predict a ~ 20 -fold increase in the nova rate of a stellar population which has formed stars continuously over a Hubble time, compared to that of a stellar population which arose in a single burst 15 Gyr ago. While the precise star formation history of M49 is unknown, we note that this galaxy is likely to have a significant number of stars younger than 5–8 Gyr (Trager et al. 2000; Cohen, Blakeslee & Côté 2003). Thus, if we scale our luminosity-specific nova rate for M49 to late-type systems like the LMC and SMC, we would expect $\nu_K \sim 30 \text{ year}^{-1} 10^{-10} L_{K\odot}$ for these galaxies. Microlensing surveys of

⁵For comparison, the unweighted mean value are $\langle \nu_K \rangle = 2.20 \pm 0.24 \text{ year}^{-1} 10^{-10} L_{K\odot}$ and $\langle \nu_K \rangle = 2.66 \pm 0.30 \text{ year}^{-1} 10^{-10} L_{K\odot}$ respectively.

these galaxies show that such extreme rates can be ruled out with high confidence, despite the large uncertainties in the measured values of η and ν_K .

8. Conclusions

We have presented the results of an *HST*/WFPC2 program designed to discover novae in M49. Nine novae, five of which with fairly complete (*i.e.*, covering both the pre- and post-maximum phases) and well-sampled light curves, were discovered in a 55-day campaign. These nine novae have been used to examine the properties of novae in early-type galaxies, measure the nova rate in M49, and assess the potential of novae as distance indicators. The main results of our study are as follows:

- Compared to the M31 and Galactic samples, M49 may be under-abundant in slow, faint novae. Moreover, the distribution of novae decline rates in M49 is statistically indistinguishable from that observed for LMC. Bearing in mind the small sample of novae on which our discussion is based, the M49 results seem to argue against a simple classification of novae in a bright, fast, disk population (which should be prevalent in the LMC) and a faint, slow, bulge population (to which all of the M49 novae should belong).
- At a distance modulus of 31.06 ± 0.10 mag, measured both using SBF and GCLF, the zero point of the Maximum Magnitude versus Rate of Decline relation for the M49 novae is consistent with that derived from a sample of two dozen Galactic novae, with distances determined using expansion parallaxes. The agreement between the M49 and M31 MMRD relations is less satisfactory, possibly owing to the large uncertainty associated with M31 internal extinction (which affects the maximum magnitude of the novae observed in this galaxy). In both cases, there seems to be a substantial difference in the shape of the MMRD relation in M49, the Milky Way and M31.
- The mean magnitude of the M49 novae 15 days after maximum is marginally consistent only with one of three proposed calibrations based on Galactic novae. Furthermore, the magnitudes of the M49 novae seem to display a smaller scatter around maximum light than at 15 days past maximum. Altogether, these results caution against an indiscriminate use of novae as distance indicators.
- The global nova rate in M49 is $\eta = 100_{-30}^{+35} \text{ year}^{-1}$, corresponding to a luminosity-specific nova rate ν_K in the range $1.7\text{--}2.5 \text{ year}^{-1} 10^{-10} L_{K\odot}$ (depending on the adopted estimate for the K -band luminosity of the galaxy). This estimate accounts for observational

incompleteness, due both to the magnitude detection limits, and to the selection criteria adopted in the detection of the variable stars. The value of ν_K measured for M49 is inconsistent with the predictions of the theoretical models, unless global differences are invoked between the novae progenitors in M49 and the Milky Way (against which the models are calibrated). The luminosity specific nova rate in M49 is fully consistent with that measured in all other galaxies for which data are available, with the possible exception of the LMC.

- Last but not least, the valuable lesson learned from our program is that, overall, obtaining reliable light curves for novae is not a trivial task. Our program consumed 24 orbits of *HST* time and led to the discovery of nine novae. For comparison, 16 orbits of *HST* time were used to discover 52 Cepheid variables and measure an 8% distance to M100, also in Virgo (Ferrarese et al. 1996). In retrospect, a few changes to our observing strategy would have been advisable. Color information would have been desirable at all epochs, and a two-day interval between subsequent exposures over the entire sequence would have aided in the measurement of the novae light curve parameters. For new programs, the Advanced Camera for Surveys (ACS) would be more suitable than WFPC2 both because of the smaller pixel size (reducing the background noise) and higher sensitivity. Although these changes would lead to a better characterization of the novae light curves, they would entail a large program, likely requiring many dozens of *HST* orbits per galaxy. Even then, the low luminosity-specific nova rate, and the apparently large scatter in the MMRD and Buscombe-de Vaucouleurs relations would ultimately limit the usefulness of novae as distance indicators. SBF has been proven to be a reliable — and efficient — indicator for early type galaxies, while the GCLF has the potential of becoming one: they both seem more worthwhile choices for measuring distances.

We thank Edward Baltz for useful discussions, and the referee, Allen Shafter, for providing very useful comments. Support for program GO-8677 was provided through a grant from the Space Telescope Science Institute, which is operated by the Association of Universities for Research in Astronomy, Inc., under NASA contract NAS5-26555. P.C. acknowledges additional support provided by NASA LTSA grant NAG5-11714. L.F. acknowledges additional support provided by NASA through LTSA grant number NRA-98-03-LTSA-03. A.J. acknowledges additional financial support provided by the National Science Foundation through a grant from the Association of Universities for Research in Astronomy, Inc., under NSF cooperative agreement AST-9613615, and by Fundación Andes under project No.C-13442.

REFERENCES

- Aaronson, M. 1978, *ApJ*, 221, L103
- Alard, C., & Lupton, R.H. 1998, *ApJ*, 503, 325
- Arp, H.C. 1956, *AJ*, 61, 15
- Baltz, E.A., & Silk, J. 2000, *ApJ*, 530, 578
- Baltz, E.A., & Silk, J. 2001, *MNRAS*, 323, 31
- Bertin, E., & Arnouts, S. 1996, *A&AS*, 117, 393
- Bianchi, L., Clayton, G.C., Bohlin, R.C., Hutchings, J.B., & Massey, P. 1996, *ApJ*, 471, 203
- Biretta, J., et al. 2001, *WFPC2 Instrument Handbook*, Version 6.0 (Baltimore: STScI).
- Buscombe, W., & de Vaucouleurs, G. 1955, *Observatory*, 75, 170
- Capaccioli, M., Della Valle, M., Rosino, L., & D’Onofrio, M. 1989, *AJ*, 97, 1622
- Capaccioli, M., Della Valle, M., Rosino, L., & D’Onofrio, M. 1990, *ApJ*, 360, 63
- Ciardullo, R., Shafter, A.W., Ford, H.C., Neill, J.D., Shara, M.M., & Tomaney, A.B. 1990, *ApJ*, 356, 472
- Cohen, J.G. 1985, *ApJ*, 292, 90
- Cohen, J.G., Blakeslee, J.P., & Côté, P. 2003, *ApJ*, in press
- Côté, P., McLaughlin, D.E., Cohen, J.G., & Blakeslee, J.P. 2003, *ApJ*, 591, 850
- Cox, A.N. 2000, *Allen’s Astrophysical Quantities* (4th ed.; New York: Springer)
- Della Valle, M., Rosino, L., Bianchini, A., & Livio, M. 1994, *A&A*, 287, 403
- Della Valle, M., & Duerbeck, H.W. 1993, *A&A*, 275, 239
- Della Valle, M., & Livio, M. 1995, *ApJ*, 452, 704
- Della Valle, M. 2002, in *Classical Nova Explosions*, ed. M. Hernanz & J. José, *A.I.P. Conference Proc.*, 443
- Della Valle, M., & Gilmozzi R. 2002, *Science*, 296, 1275
- Downes, R.A., & Duerbeck, H.W. 2000, *AJ*, 120, 2007

- Duerbeck, H.W. 1981, *PASP*, 93, 165
- Duerbeck, H.W. 1990, in *IAU Colloq. 122, Physics of Classical Novae*, ed. A. Cassatella & R. Viotti (Berlin: Springer), 34
- Ferrarese, L., Livio, M., Freedman, W., Saha, A., Stetson, P.B., Ford, H.C., Hill, R.J., & Madore, B.F. 1996, *ApJ*, 468, 95
- Ferrarese, L., et al. 2000, *ApJ*, 529, 745
- Frogel, J.A., Persson, S.E., Matthews, K., & Aaronson, M. 1978, *ApJ*, 220, 75
- Graham, J.A. 1979, in *IAU Colloq. 46, Changing Trends in Variable Star Research*, ed. F.M. Bateson, J. Smak, & I.H. Urch (Hamilton: Univ. Waikato), 96
- Hamuy, M., Phillips, M.M., Suntzeff, N.B., Schommer, R.A., Maza, J., Smith, R.C., Lira, P., & Aviles, R. 1996, *AJ*, 112, 2438
- Harris, W.E. 2001, in *Star Clusters, Saas-Fee Advanced School 28*, ed. L. Labhardt & B. Binggeli (Berlin: Springer), 223
- Hill, R., et al. 1998, *ApJ*, 496, 648
- Hoffmeister, C., Richter, G., & Wenzel, W. 1984, *Variable Stars*, (Berlin: Springer)
- Holtzman, J.A., Burrows, C.J., Casertano, S., Hester, J.J., Trauger, J.T., Watson, A.M., & Worthey, G. 1995, *PASP*, 107, 1065
- Hubble, E.P. 1929, *ApJ*, 69, 103
- Jacoby, G.H., et al. 1992, *PASP*, 104, 599
- Jarrett, T.H., Chester, T., Cutri, R., Schneider, S.E., & Huchra, J.P. 2003, *AJ*, 125, 525
- Larsen, S.S., Brodie, J.P., Huchra, J.P., Forbes, D.A., & Grillmair, Carl J. 2001, *AJ*, 121, 2974
- Livio, M. 1992, *ApJ*, 393, 516
- Matteucci, F., Renda, A., Pipino, A., & Della Valle, M. 2003, *A&A*, 405, 23
- McLaughlin, D.B. 1945, *PASP*, 57, 69
- Moses, R.N., & Shafter, A.W. 1993, *BAAS*, 25, 1248

- Nobili, S., Goobar, A., Knop, R., & Nugent, P. 2003, *A&A*, 404, 901
- Pain, R., et al. 2002, *ApJ*, 577, 132
- Peterson, B.M. 2001, in *Advanced Lectures on the Starburst-AGN Connection*, eds Itziar Aretxaga, Daniel Kunth, and Raúl Mújica. Singapore: World Scientific, p.3
- Pritchett, C.J., & van den Bergh, S. 1985, *ApJ*, 288, L41
- Pritchett, C.J., & van den Bergh, S. 1987, *ApJ*, 318, 507
- Ritchey, G.W. 1917, *PASP*, 29, 210
- Rosino, M. 1973, *A&AS*, 9, 347
- Rosino, M., Capaccioli, M., D’Onofrio, M., & Della Valle, M. 1989, *AJ*, 97, 83
- Saha, A., et al. 1994, *ApJ*, 425, 14
- Saha, A., et al. 1996, *ApJ*, 466, 55
- Schechter, P.L., Mateo, M., & Saha, A. 1993, *PASP*, 105, 1342
- Schlegel, D.J., Finkbeiner, D.P., & Davis, M. 1998, *ApJ*, 500, 525
- Schmidt, B., et al. 1998, *ApJ*, 507, 46
- Shafter, A.W., Ciardullo, R., & Pritchett, C.J. 2000, *ApJ*, 530, 193
- Shafter, A.W., & Irby, B.K. 2001, *ApJ*, 563, 749
- Shapley, H. 1917, *PASP*, 29, 213
- Shara, M.M., & Zurek, D.R. 2002, in *Classical Nova Explosions*, ed. M. Hernanz & J. José, A.I.P. Conference Proc., 457
- Shara, M.M. 1981a, *ApJ*, 243, 926
- Shara, M.M. 1981b, *ApJ*, 243, 268
- Sharov, A.S. 1993, *Astron. Lett.*, 19, 147
- Starck, J.-L., Murtagh, F., & Bijaoui, A. 1998, *Image Processing and Data Analysis* (Cambridge: Cambridge University Press)
- Stetson, P.B., et al. 1998, *ApJ*, 508, 491

Stetson, P.B. 1998, PASP, 110,1448

Tonry, J.L., Dressler, A., Blakeslee, J.P., Ajhar, E.A., Fletcher, A.B., Luppino, G.A., Metzger, M.R., & Moore, C.B. 2001, ApJ, 546, 681

Trager, S.C., Faber, S.M., Worthey, G., González, J.J. 2000, AJ, 120, 165

van den Bergh, S., & Younger, F. 1987, A&AS, 70, 125

Yungelson, L., Livio, M., & Tutukov, A. 1997, ApJ, 481, 127

Zombeck, M.V. 1990, Handbook of Space Astronomy and Physics (2d ed.; Cambridge: Cambridge Univ. Press)

Zwicky, F. 1936, PASP, 48, 191

NOTE: FIGURES 1 TO 7 ARE NOT INCLUDED IN THIS SUBMISSION BECAUSE OF SPACE LIMITATIONS. THEY ARE INCLUDED IN THE PDF VERSION OF THIS PAPER WHICH CAN BE FOUND AT <http://www.physics.rutgers.edu/~lff/publications.html>

Fig. 1.— Digitized sky survey image of M49 showing the location and orientation of our WFPC2 fields. The image measures $6' \times 6'$.

Fig. 2.— *HST*/WFPC2 image of M49. This F555W image shows the WF2 field, with the positions of novae #1–5 indicated.

Fig. 3.— *HST*/WFPC2 image of M49. This F555W image shows the WF3 field, with the positions of novae #6 and 7 indicated.

Fig. 4.— *HST*/WFPC2 image of M49. This F555W image shows the WF4 field, with the positions of novae #8 and 9 indicated.

Fig. 5.— The location of the nine novae discovered in M49, superimposed on an isophotal contour of the galaxy. The isophotes are drawn at 0.5 mag/arcsec^2 intervals, from $\mu_V = 16 \text{ mag/arcsec}^2$ to $\mu_V = 20.5 \text{ mag/arcsec}^2$. The WFPC2 footprint is also shown. The image is $2''.7$ on the side, and has the same orientation as Figure 1 (N at the top and E to the left).

Fig. 6.— Appearance of novae #1–5 at five different epochs. Each panel shows a $2''.7 \times 2''.7$ region centered on the nova, in the F555W bandpass. Epoch numbers are indicated in each panel.

Fig. 7.— Appearance of novae #6–9 at five different epochs. Each panel shows a $2''.7 \times 2''.7$ region centered on the nova, in the F555W bandpass. Epoch numbers are indicated in each panel.

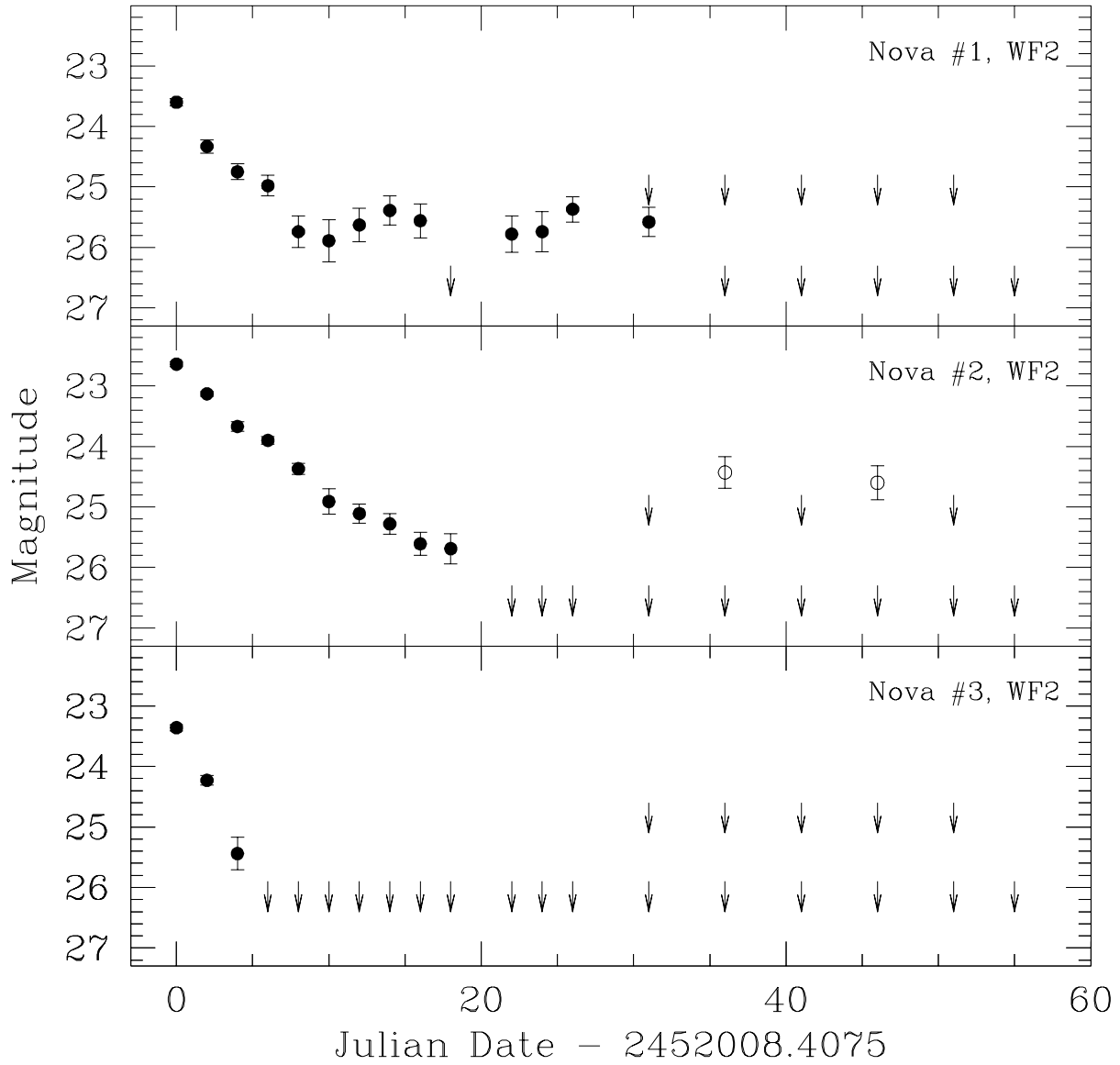


Fig. 8.— Light curves for novae #1, 2 and 3 in V (filled symbols) and I (open symbols). The lower and upper arrows show respective upper limits on the V and I magnitudes at epochs where the novae were undetected.

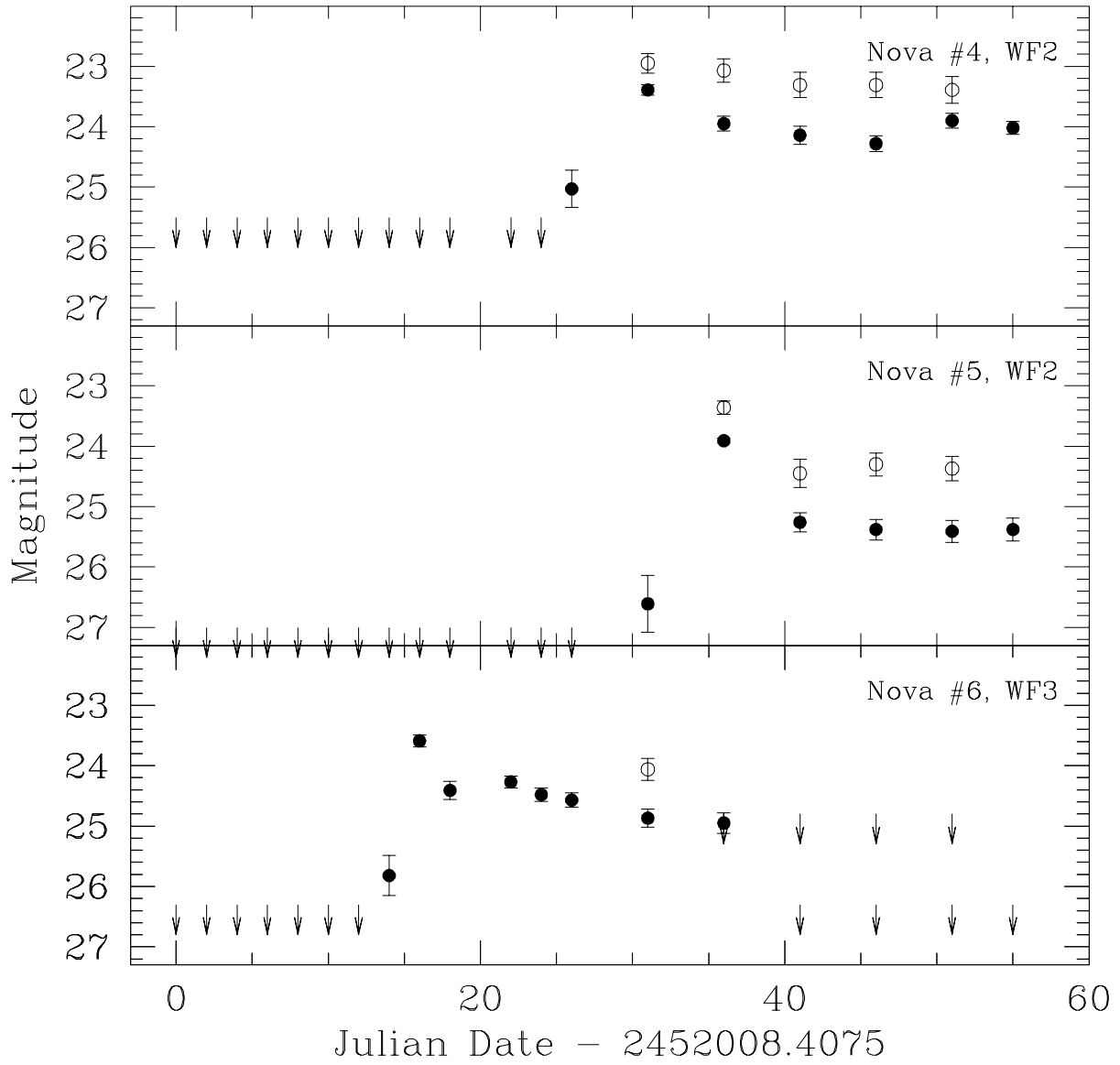


Fig. 9.— Same as Figure 8 except for novae #4, 5 and 6.

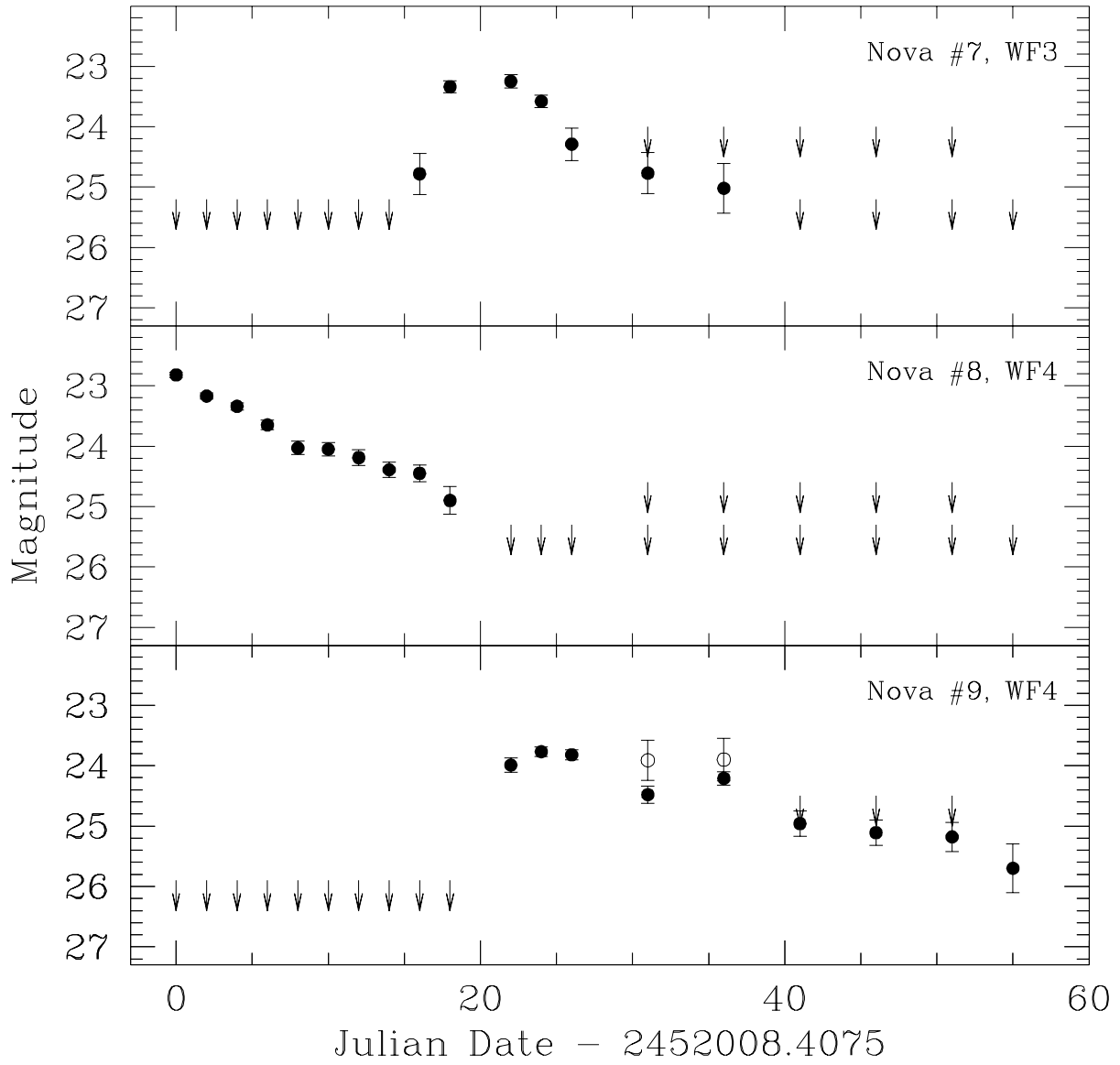


Fig. 10.— Same as Figure 8 except for novae #7, 8 and 9.

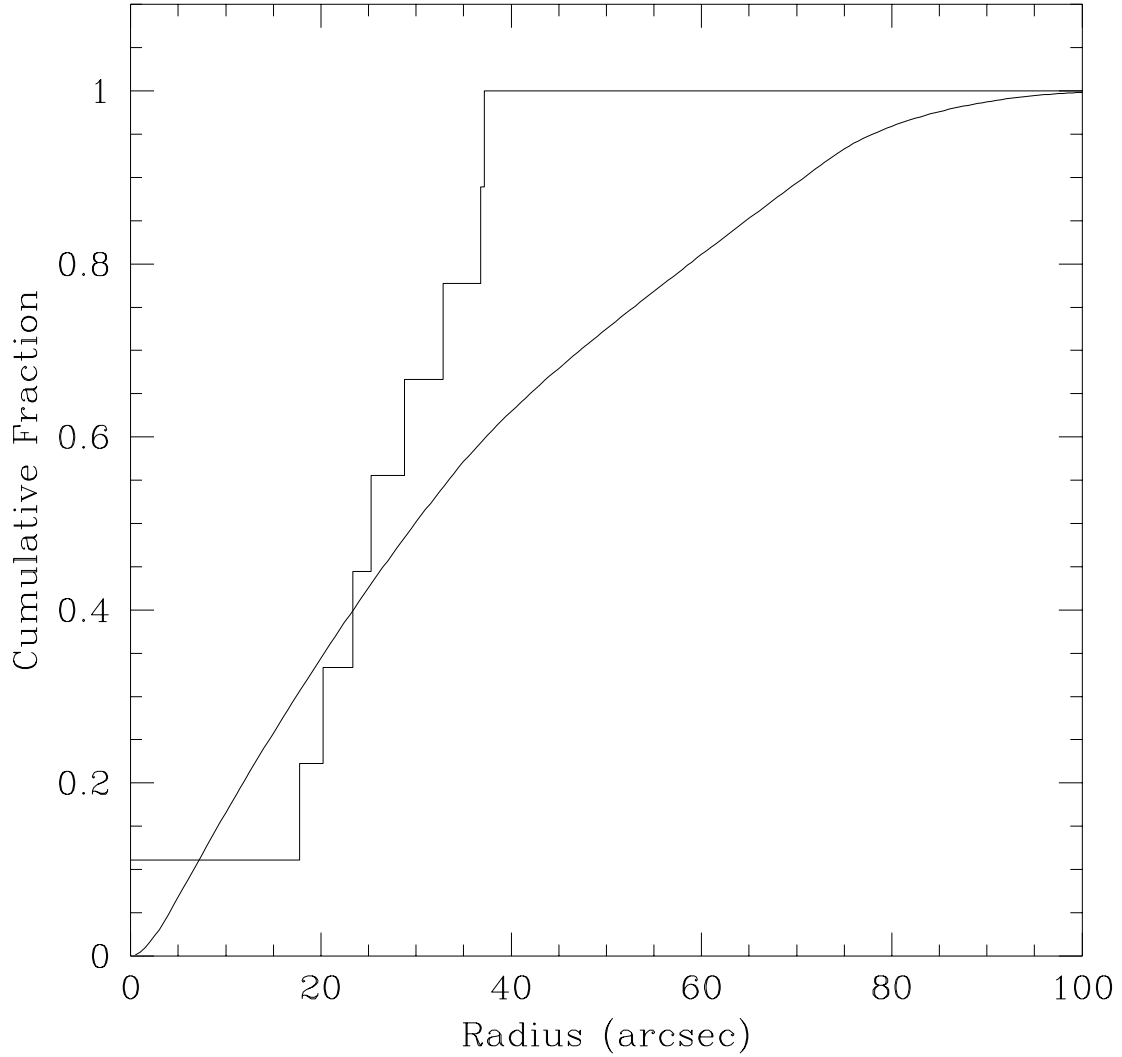


Fig. 11.— A comparison between the cumulative distribution of the novae detected in M49 and the cumulative fraction of the underlying galaxy V -band light, normalized to the total light within the WFPC2 field. As is evident from Figures 2-5, the novae appear to be more centrally concentrated than the galaxy light.

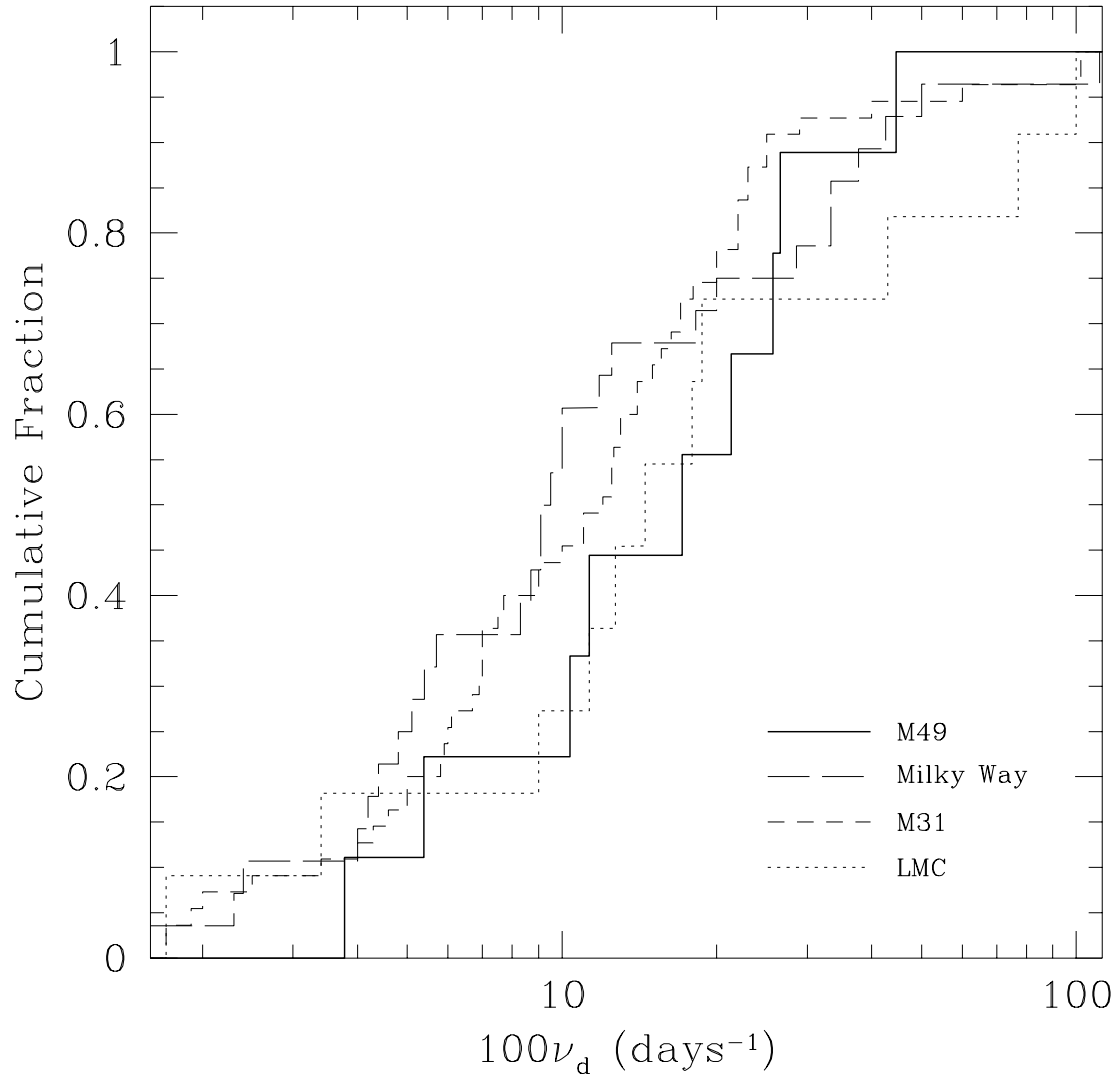


Fig. 12.— The cumulative fraction of M31, LMC, Milky Way, and M49 novae as a function of decline rate, defined as $\nu_d = 2/t_2$, where t_2 is the time it takes for the nova to decline by 2 magnitudes (in V -band) after reaching maximum light. The LMC and M49 samples are statistically indistinguishable.

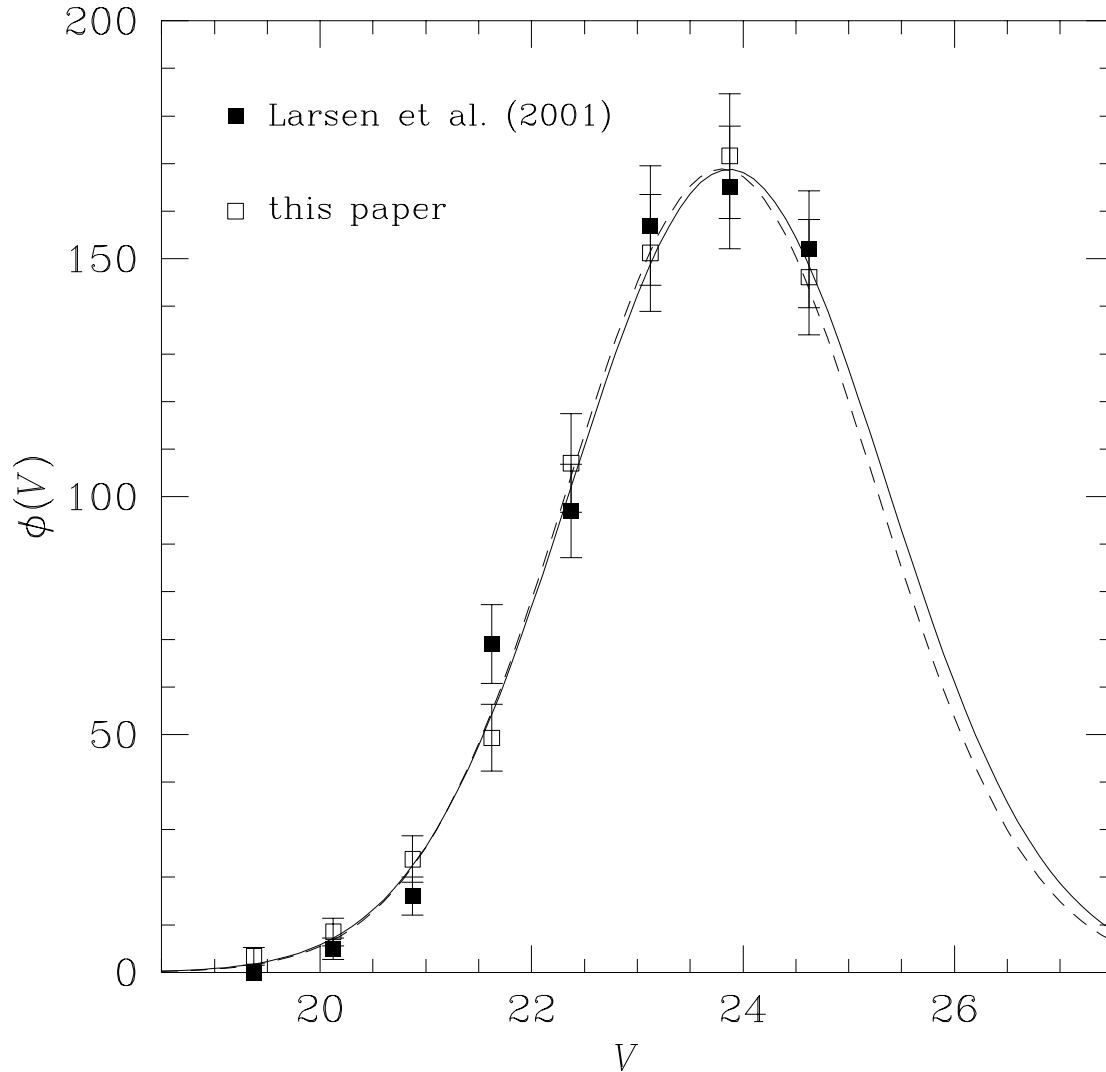


Fig. 13.— Globular cluster luminosity function, $\phi(V)$, for M49. Filled symbols indicate the luminosity function of Larsen et al. (2001). Open symbols show the luminosity function determined from our deep V and I images, scaled upwards by a factor $(661/389) \approx 1.7$. The solid curve shows an unconstrained Gaussian fit to the luminosity function derived from our observations; the apparent magnitude of the turnover is $V^{\text{TO}} = 23.87 \pm 0.06$. The dashed curve shows the best-fit obtained when the apparent turnover magnitude is fixed at $V^{\text{TO}} = 23.80$; this is the value expected on the basis of the SBF distance modulus, $(m - M)_0 = 31.06 \pm 0.10$ (Tonry et al. 2001), and the absolute value of $M_V^{\text{TO}} = -7.33 \pm 0.04$ given in Harris (2001).

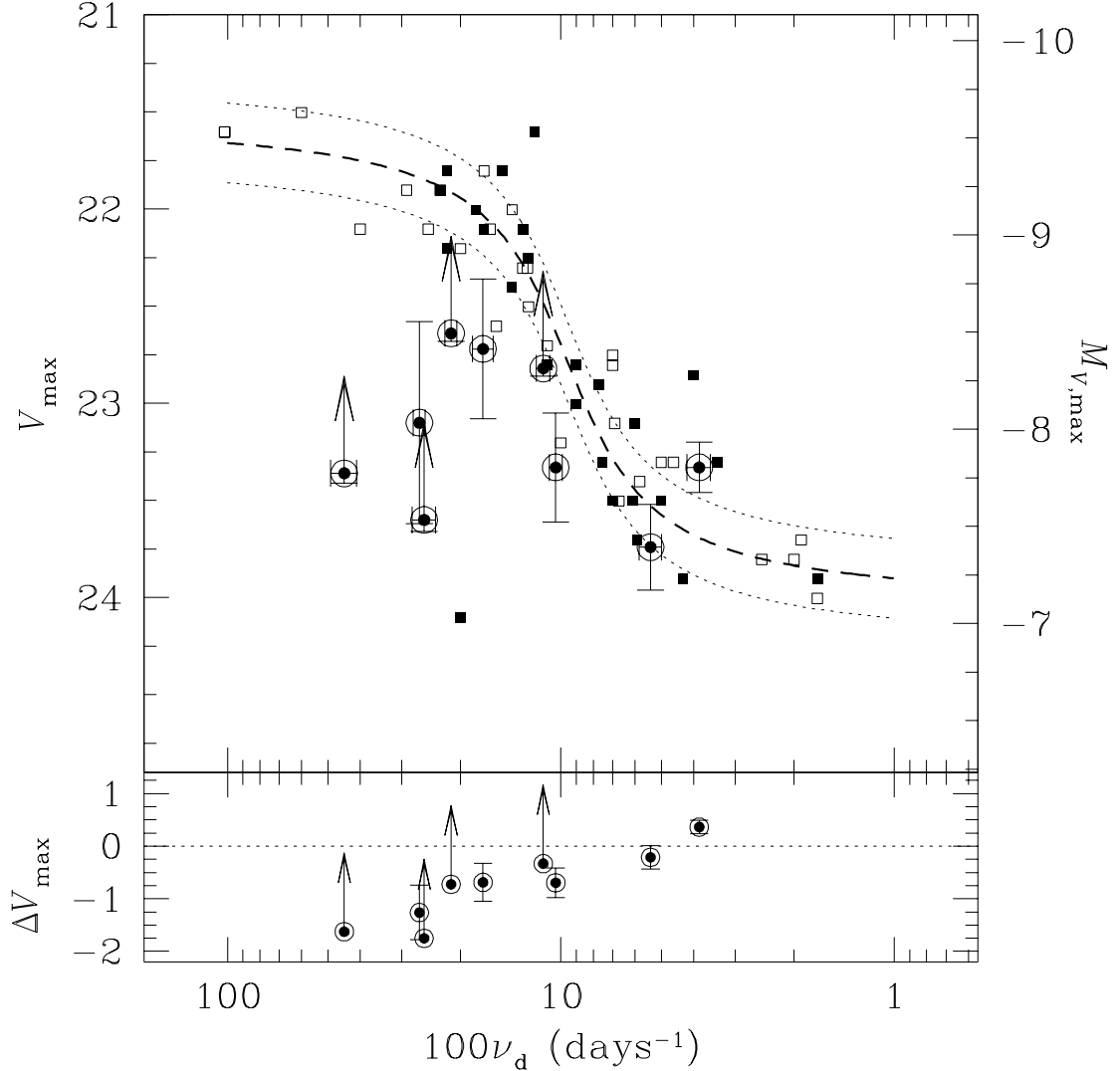


Fig. 14.— The Maximum Magnitude versus Rate of Decline (MMRD) relation for the M49 novae, shown as circled symbols. Filled and open squares show M31 novae judged by Capaccioli et al. (1989) to have light curves of good and fair quality, respectively; their apparent magnitudes have been scaled to the distance and reddening of M49. The thick dashed curve shows the best fit MMRD relation for M31 (from Capaccioli et al. 1989, again shifted to the distance of M49), with 1σ uncertainties shown by the thin dotted curves. Absolute magnitudes are shown at right under the assumption that $(m - M)_0 = 31.06 \pm 0.10$ mag and $A(V) = 0.07$ mag for M49. The lower panel shows the deviations of the M49 novae from the M31 MMRD relation.

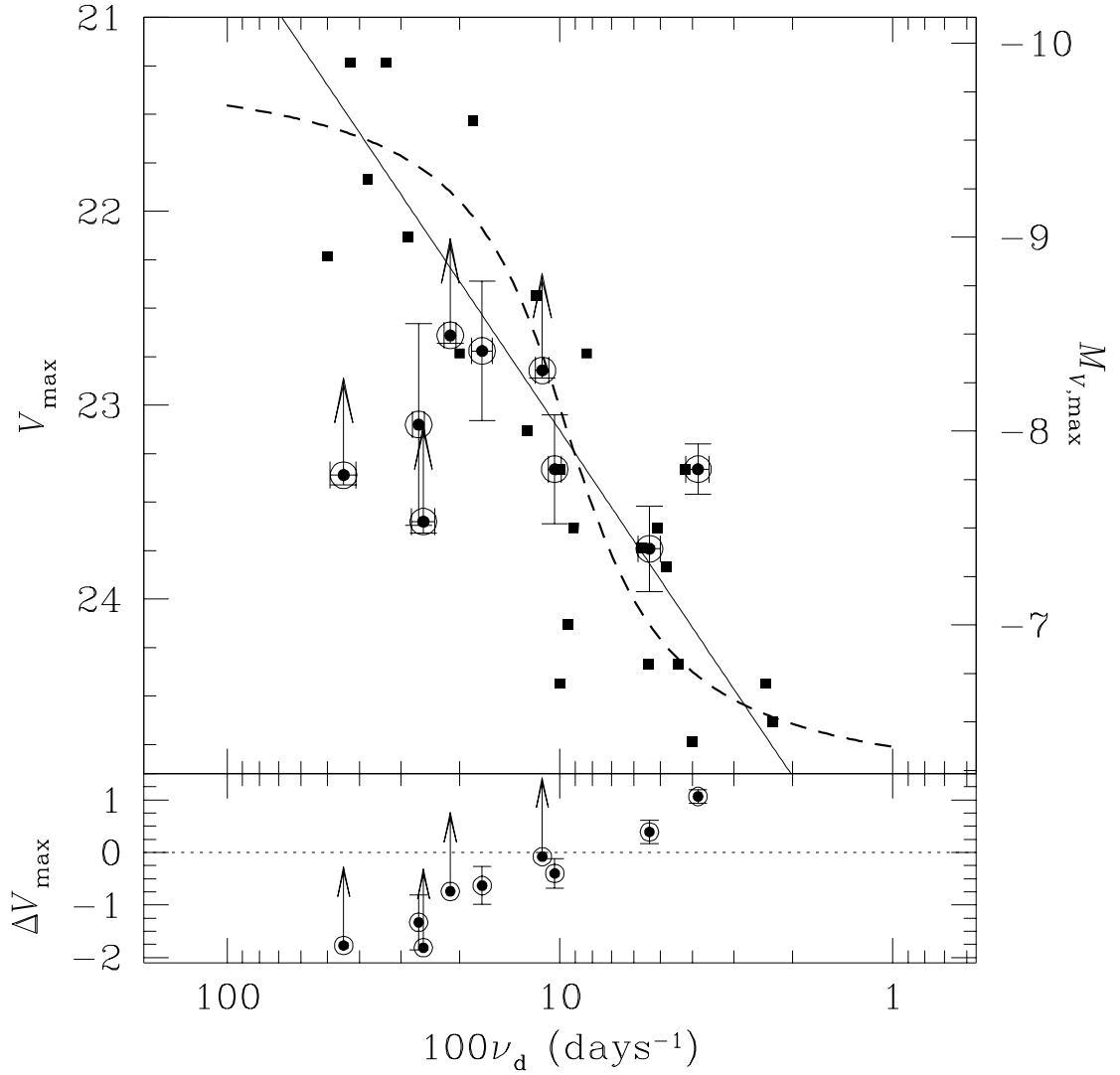


Fig. 15.— Same as Figure 14, except the comparison is now between the M49 (circled symbols) and Galactic novae (filled squares). The dashed and solid curves are the best fit “S-shaped” and power law fits to the Galactic novae from Downes & Duerbeck (2000); residuals between the former and the M49 novae are shown in the lower panel.

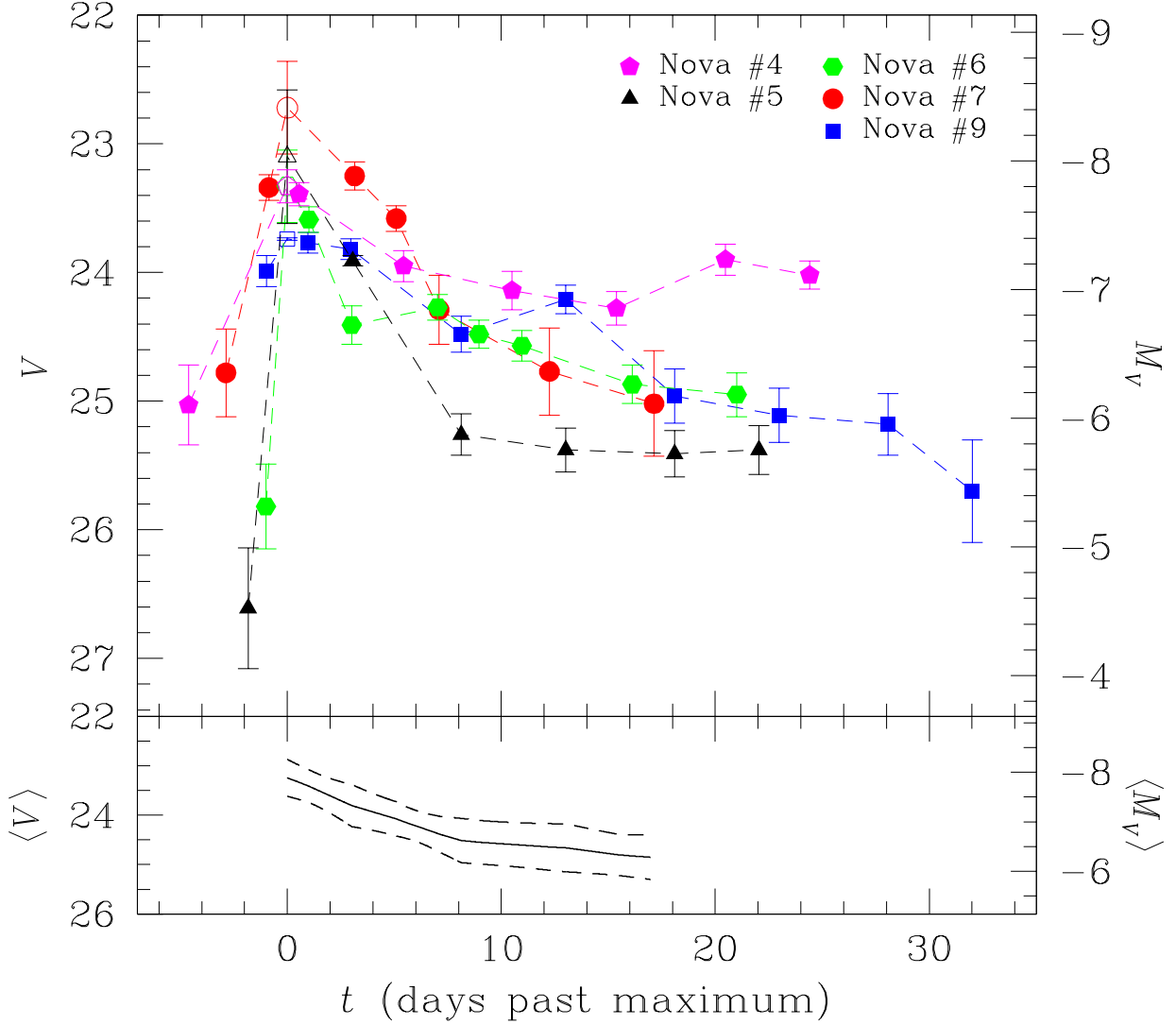


Fig. 16.— (*Upper Panel*) Light curves for the five M49 novae having measured V_{\max} and t_{\max} . The light curves have been shifted so that the times of maximum light align. Observed values are shown as filled symbols; open symbols indicate our best estimates for V_{\max} . The novae have $V_{15} = 24.77 \pm 0.19$ at 15 days past maximum, corresponding to $M_{V,15} = -6.36 \pm 0.19$. The standard deviation about this mean value is $\sigma \simeq 0.43$. (*Lower Panel*) The mean magnitude averaged over the five novae plotted in the upper panel, as a function of time following maximum.

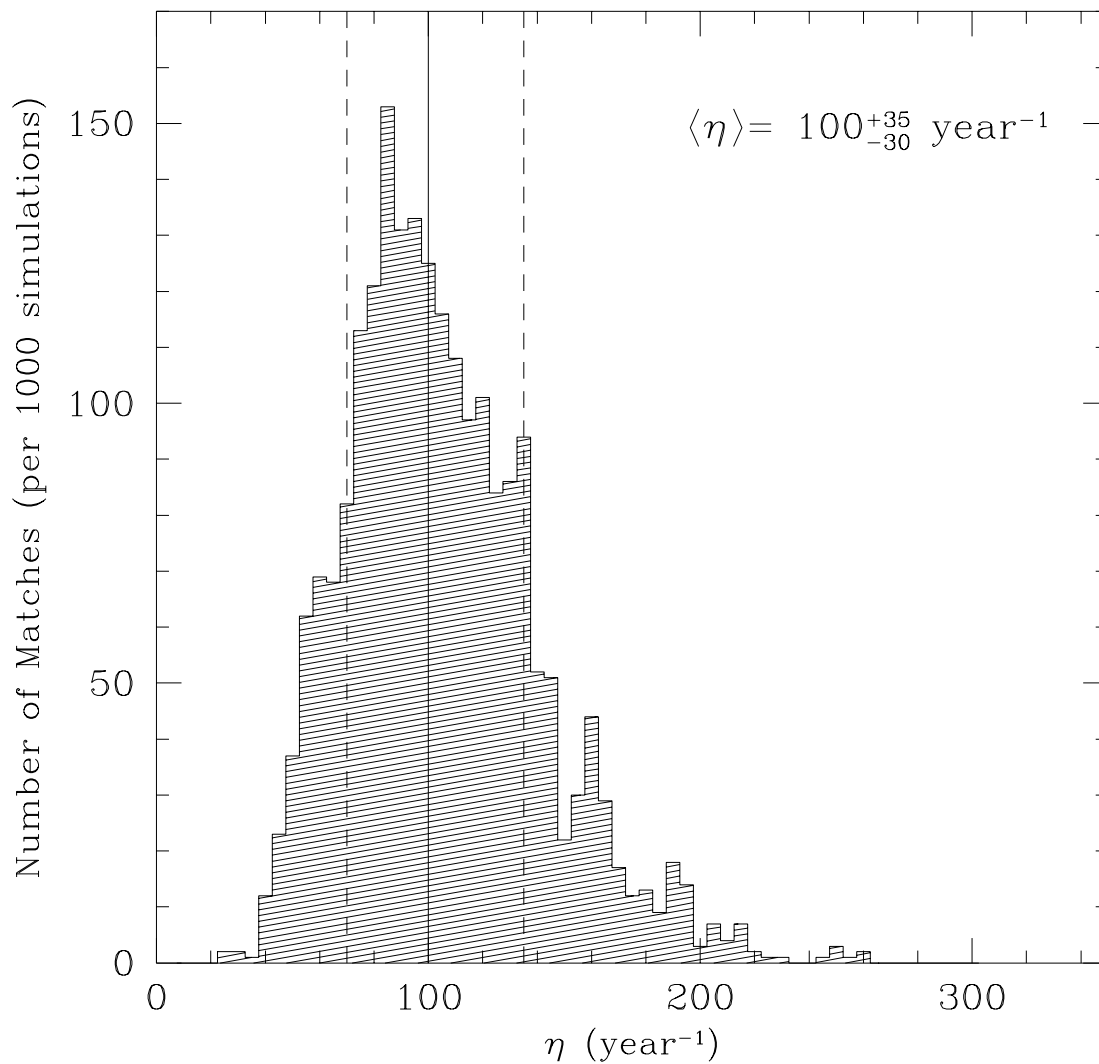


Fig. 17.— Monte Carlo simulations of the global nova rate in M49. The histogram gives the number of times — based on 1000 simulations at each η — that the simulated datasets contained exactly nine novae that would have been discovered using our observing strategy and data reduction procedures. The solid and dashed lines show our best estimates for the global nova rate and its $1\text{-}\sigma$ uncertainties: $\eta = 100_{-30}^{+35} \text{ year}^{-1}$.

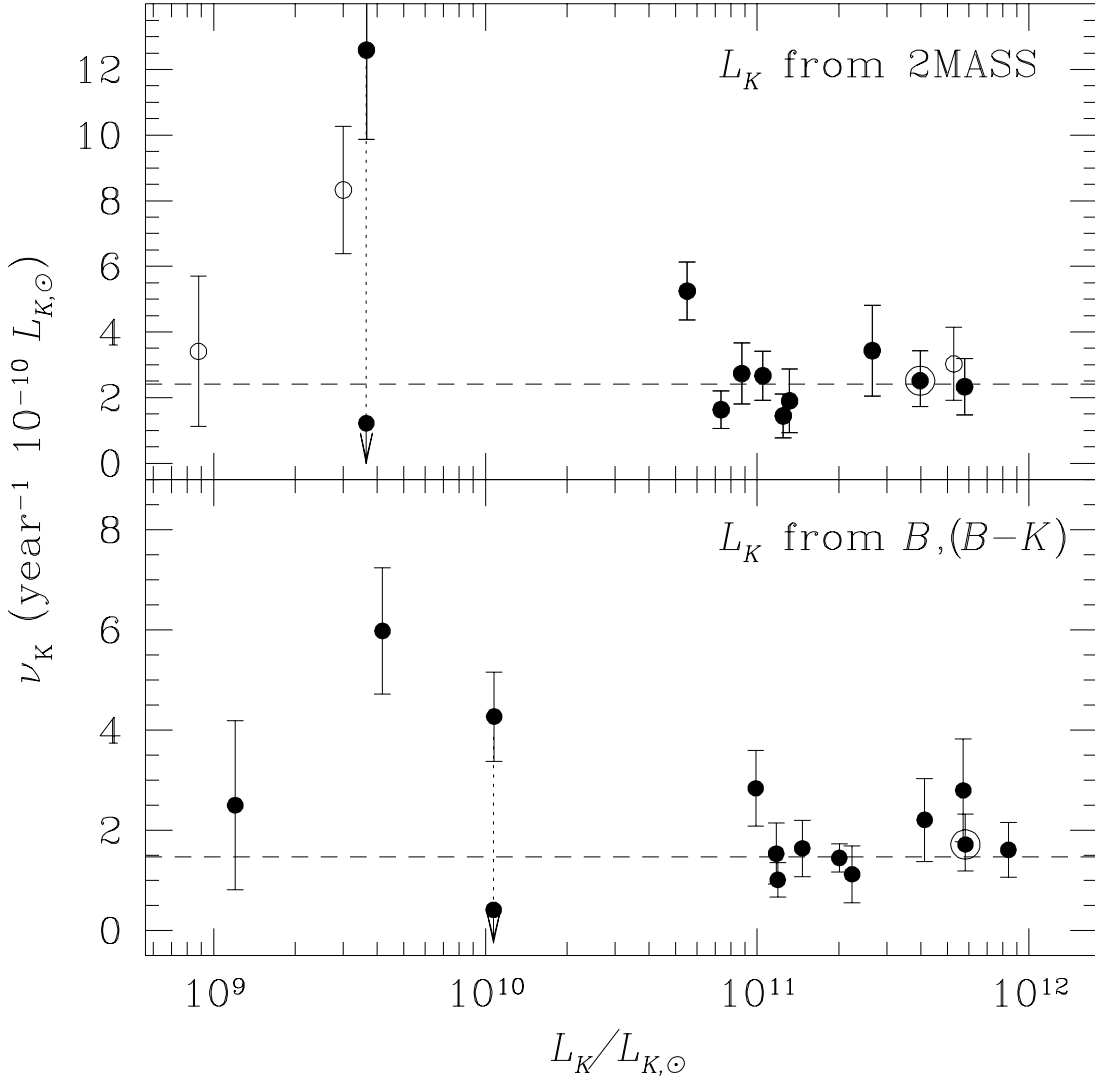


Fig. 18.— Luminosity-specific nova rates, ν_K , for all galaxies with measured global nova rates. The global nova rates have been normalized by the total K -band luminosity of each galaxy, derived from 2MASS (upper panel - the open circles denote galaxies for which 2MASS magnitudes are not available, and K -band magnitudes were derived from the RC3 B -band magnitudes as in the lower panel) or inferred from the RC3 B -band magnitudes via a color correction (lower panel – see text for further details). M49 is indicated by the circled point. For M33, two different — and inconsistent — estimates of the nova rate are available (see text for details). The dashed line shows the weighted mean, excluding M33: $\bar{\nu}_K = 1.58 \pm 0.16 \text{ year}^{-1} 10^{-10} L_{K,\odot}$ in the lower panel, $\bar{\nu}_K = 2.41 \pm 0.27 \text{ year}^{-1} 10^{-10} L_{K,\odot}$ in the upper panel.

Table 1. Log of Observations GO-8677

Epoch	Observation Date	Julian Date ^a (2,400,000+)	Dataset Name	Exposure Time (seconds)	Filter
1	2001 Apr 9	52008.39844	U6630101R	1200	F555W
1	2001 Apr 9	52008.41406	U6630102R	1200	F555W
2	2001 Apr 11	52010.47266	U6630201R	1200	F555W
2	2001 Apr 11	52010.48438	U6630202R	1200	F555W
3	2001 Apr 13	52012.47656	U6630301R	1200	F555W
3	2001 Apr 13	52012.49219	U6630302R	1200	F555W
4	2001 Apr 15	52014.48438	U6630401R	1200	F555W
4	2001 Apr 15	52014.50000	U6630402R	1200	F555W
5	2001 Apr 17	52016.49219	U6630501R	1200	F555W
5	2001 Apr 17	52016.50781	U6630502R	1200	F555W
6	2001 Apr 19	52018.50000	U6630601R	1200	F555W
6	2001 Apr 19	52018.51562	U6630602R	1200	F555W
7	2001 Apr 21	52020.50391	U6630701R	1200	F555W
7	2001 Apr 21	52020.52344	U6630702M	1200	F555W
8	2001 Apr 23	52022.44141	U6630801R	1200	F555W
8	2001 Apr 23	52022.46094	U6630802R	1200	F555W
9	2001 Apr 25	52024.45312	U6630901R	1200	F555W
9	2001 Apr 25	52024.47266	U6630902R	1200	F555W
10	2001 Apr 27	52026.46094	U6631001R	1200	F555W
10	2001 Apr 27	52026.47656	U6631002R	1200	F555W
11	2001 May 1	52030.47656	U6631201R	1200	F555W
11	2001 May 1	52030.48828	U6631202R	1200	F555W
12	2001 May 3	52032.41016	U6631301R	1200	F555W
12	2001 May 3	52032.42578	U6631302R	1200	F555W
13	2001 May 5	52034.41797	U6631401R	1200	F555W
13	2001 May 5	52034.43359	U6631402R	1200	F555W
14	2001 May 10	52039.57422	U6631501R	1200	F555W
14	2001 May 10	52039.58594	U6631502R	1200	F555W
14	2001 May 10	52039.63281	U6631503R	1300	F814W
14	2001 May 10	52039.64844	U6631504R	1300	F814W

Table 1—Continued

Epoch	Observation Date	Julian Date ^a (2,400,000+)	Dataset Name	Exposure Time (seconds)	Filter
15	2001 May 15	52044.46094	U6631601R	1200	F555W
15	2001 May 15	52044.48047	U6631602M	1200	F555W
15	2001 May 15	52044.52734	U6631603R	1300	F814W
15	2001 May 15	52044.54297	U6631604R	1300	F814W
16	2001 May 20	52049.54297	U6631701R	1200	F555W
16	2001 May 20	52049.56250	U6631702R	1200	F555W
16	2001 May 20	52049.60938	U6631703R	1300	F814W
16	2001 May 20	52049.62500	U6631704R	1300	F814W
17	2001 May 25	52054.42578	U6631801R	1200	F555W
17	2001 May 25	52054.44531	U6631802R	1200	F555W
17	2001 May 25	52054.49219	U6631803R	1300	F814W
17	2001 May 25	52054.50781	U6631804R	1300	F814W
18	2001 May 30	52059.50781	U6631901R	1200	F555W
18	2001 May 30	52059.52344	U6631902R	1200	F555W
18	2001 May 30	52059.57812	U6631903R	1300	F814W
18	2001 May 30	52059.58984	U6631904R	1300	F814W
19	2001 Jun 3	52063.45312	U6631101R	1200	F555W
19	2001 Jun 3	52063.47266	U6631102R	1200	F555W

^aModified Julian date at the middle of the exposure.

Table 2. Coordinates of Novae in M49

Nova	α (J2000)	δ (J2000)	R (arcsec)
1	12:29:45.286	7:59:42.73	28.79
2	12:29:45.087	7:59:39.95	32.84
3	12:29:45.116	7:59:54.95	25.26
4	12:29:46.102	7:59:46.61	17.74
5	12:29:44.484	7:59:45.93	37.19
6	12:29:46.279	8:00:37.51	36.78
7	12:29:46.428	8:00:15.15	14.57
8	12:29:47.246	8:00:20.35	20.25
9	12:29:47.277	8:00:23.48	23.36

Note. — Units of right ascension are hours, minutes, and seconds, and units of declination are degrees, arcminutes, and arcseconds. R is the distance of the nova from the center of M49.

Table 3. Novae Photometry

Epoch	Julian Date	Nova 1		Nova 2		Nova 3		Nova 4	
		<i>V</i>	<i>I</i>	<i>V</i>	<i>I</i>	<i>V</i>	<i>I</i>	<i>V</i>	<i>I</i>
1	2452008.4075	23.60±0.06	...	22.64±0.04	...	23.36±0.05	...	≥25.50	...
2	2452010.4818	24.33±0.11	...	23.13±0.04	...	24.23±0.08	...	≥25.50	...
3	2452012.4887	24.75±0.13	...	23.67±0.08	...	25.44±0.27	...	≥25.50	...
4	2452014.4964	24.98±0.17	...	23.90±0.06	...	≥25.90	...	≥25.50	...
5	2452016.5033	25.74±0.26	...	24.37±0.09	...	≥25.90	...	≥25.50	...
6	2452018.5102	25.89±0.35	...	24.91±0.21	...	≥25.90	...	≥25.50	...
7	2452020.5179	25.63±0.28	...	25.11±0.16	...	≥25.90	...	≥25.50	...
8	2452022.4575	25.39±0.24	...	25.28±0.17	...	≥25.90	...	≥25.50	...
9	2452024.4644	25.56±0.28	...	25.61±0.19	...	≥25.90	...	≥25.50	...
10	2452026.4713	≥26.30	...	25.69±0.25	...	≥25.90	...	≥25.50	...
11	2452030.4846	25.78±0.30	...	≥26.30	...	≥25.90	...	≥25.50	...
12	2452032.4248	25.74±0.33	...	≥26.30	...	≥25.90	...	≥25.50	...
13	2452034.4318	25.37±0.21	...	≥26.30	...	≥25.90	...	25.03±0.31	...
14	2452039.5863	25.58±0.24	≥24.80	≥26.30	≥24.80	≥25.90	≥24.60	23.39±0.09	22.95±0.16
15	2452044.4706	≥26.30	≥24.80	≥26.30	24.43±0.26	≥25.90	≥24.60	23.95±0.12	23.07±0.19
16	2452049.5547	≥26.30	≥24.80	≥26.30	≥24.80	≥25.90	≥24.60	24.14±0.15	23.31±0.21
17	2452054.4373	≥26.30	≥24.80	≥26.30	24.60±0.28	≥25.90	≥24.60	24.28±0.13	23.31±0.21
18	2452059.5207	≥26.30	≥24.80	≥26.30	≥24.80	≥25.90	≥24.60	23.90±0.12	23.39±0.22
19	2452063.4651	≥26.30	...	≥26.30	...	≥25.90	...	24.02±0.11	...

Table 4. Novae Photometry

Epoch	Julian Date	Nova 5		Nova 6		Nova 7		Nova 8	
		<i>V</i>	<i>I</i>	<i>V</i>	<i>I</i>	<i>V</i>	<i>I</i>	<i>V</i>	<i>I</i>
1	2452008.4075	≥ 27.00	...	≥ 26.30	...	≥ 25.20	...	22.82 ± 0.04	...
2	2452010.4818	≥ 27.00	...	≥ 26.30	...	≥ 25.20	...	23.17 ± 0.05	...
3	2452012.4887	≥ 27.00	...	≥ 26.30	...	≥ 25.20	...	23.34 ± 0.06	...
4	2452014.4964	≥ 27.00	...	≥ 26.30	...	≥ 25.20	...	23.65 ± 0.08	...
5	2452016.5033	≥ 27.00	...	≥ 26.30	...	≥ 25.20	...	24.03 ± 0.11	...
6	2452018.5102	≥ 27.00	...	≥ 26.30	...	≥ 25.20	...	24.05 ± 0.11	...
7	2452020.5179	≥ 27.00	...	≥ 26.30	...	≥ 25.20	...	24.19 ± 0.13	...
8	2452022.4575	≥ 27.00	...	25.82 ± 0.83	...	≥ 25.20	...	24.39 ± 0.13	...
9	2452024.4644	≥ 27.00	...	23.59 ± 0.10	...	24.78 ± 0.34	...	24.45 ± 0.14	...
10	2452026.4713	≥ 27.00	...	24.41 ± 0.15	...	23.34 ± 0.10	...	24.90 ± 0.23	...
11	2452030.4846	≥ 27.00	...	24.27 ± 0.10	...	23.25 ± 0.11	...	≥ 25.30	...
12	2452032.4248	≥ 27.00	...	24.48 ± 0.11	...	23.58 ± 0.10	...	≥ 25.30	...
13	2452034.4318	≥ 27.00	...	24.57 ± 0.12	...	24.29 ± 0.27	...	≥ 25.30	...
14	2452039.5863	26.61 ± 0.47	≥ 25.10	24.87 ± 0.15	24.06 ± 0.18	24.77 ± 0.34	≥ 24.00	≥ 25.30	≥ 24.60
15	2452044.4706	23.91 ± 0.04	23.36 ± 0.11	24.95 ± 0.17	≥ 24.80	25.02 ± 0.41	≥ 24.00	≥ 25.30	≥ 24.60
16	2452049.5547	25.26 ± 0.16	24.45 ± 0.23	≥ 26.30	≥ 24.80	≥ 25.20	≥ 24.00	≥ 25.30	≥ 24.60
17	2452054.4373	25.38 ± 0.17	24.30 ± 0.19	≥ 26.30	≥ 24.80	≥ 25.20	≥ 24.00	≥ 25.30	≥ 24.60
18	2452059.5207	25.41 ± 0.18	24.37 ± 0.20	≥ 26.30	≥ 24.80	≥ 25.20	≥ 24.00	≥ 25.30	≥ 24.60
19	2452063.4651	25.38 ± 0.19	...	≥ 26.30	...	≥ 25.20	...	≥ 25.30	...

Table 5. Novae Photometry

Epoch	Julian Date	Nova 9	
		<i>V</i>	<i>I</i>
1	2452008.4075	≥ 25.90	...
2	2452010.4818	≥ 25.90	...
3	2452012.4887	≥ 25.90	...
4	2452014.4964	≥ 25.90	...
5	2452016.5033	≥ 25.90	...
6	2452018.5102	≥ 25.90	...
7	2452020.5179	≥ 25.90	...
8	2452022.4575	≥ 25.90	...
9	2452024.4644	≥ 25.90	...
10	2452026.4713	≥ 25.90	...
11	2452030.4846	23.99 ± 0.12	...
12	2452032.4248	23.77 ± 0.08	...
13	2452034.4318	23.82 ± 0.08	...
14	2452039.5863	24.48 ± 0.14	23.91 ± 0.33
15	2452044.4706	24.21 ± 0.11	23.90 ± 0.35
16	2452049.5547	24.96 ± 0.21	≥ 24.50
17	2452054.4373	25.11 ± 0.21	≥ 24.50
18	2452059.5207	25.18 ± 0.24	≥ 24.50
19	2452063.4651	25.70 ± 0.40	...

Table 6. Properties of Light Curves for Novae in M49

Nova	t_{\max} (Julian Date)	V_{\max} (mag)	$M_{V,\max}$ (mag)	t_2 (days)	ν_d (days ⁻¹)
1	≤ 2452008.4075	$\leq 23.60 \pm 0.06$	$\leq -7.53 \pm 0.12$	7.78 ± 0.62	0.257 ± 0.020
2	≤ 2452008.4075	$\leq 22.64 \pm 0.04$	$\leq -8.49 \pm 0.11$	9.37 ± 0.38	0.213 ± 0.009
3	≤ 2452008.4075	$\leq 23.36 \pm 0.05$	$\leq -7.77 \pm 0.11$	4.48 ± 0.40	0.446 ± 0.040
4	2452039.04 ± 1.11	23.33 ± 0.13	-7.80 ± 0.16	52.00 ± 4.21	0.038 ± 0.003
5	2452041.42 ± 1.95	23.10 ± 0.52	-8.03 ± 0.53	7.53 ± 1.14	0.266 ± 0.011
6	2452023.46 ± 0.50	23.33 ± 0.28	-7.80 ± 0.30	19.30 ± 0.86	0.104 ± 0.005
7	2452027.33 ± 0.50	22.72 ± 0.36	-8.41 ± 0.37	11.68 ± 0.83	0.171 ± 0.012
8	≤ 2452008.4075	$\leq 22.82 \pm 0.04$	$\leq -8.31 \pm 0.11$	17.71 ± 0.81	0.113 ± 0.005
9	2452031.45 ± 0.50	23.74 ± 0.22	-7.39 ± 0.24	37.16 ± 2.86	0.054 ± 0.004

Table 7. Absolute and Normalized Nova Rates

Galaxy	T	η^a (year ⁻¹)	B (mag)	K_{2MASS} (mag)	$(B - K)_0^b$ (mag)	$A(B)_i^c$ (mag)	$A(B)_g^c$ (mag)	$(m - M)^d$ (mag)	$\nu_{K,B}$ (year ⁻¹ 10 ⁻¹⁰ L _{K\odot})	$\nu_{K,2MASS}$ (year ⁻¹ 10 ⁻¹⁰ L _{K\odot})
LMC	9	2.5±0.5	0.91±0.05	...	2.74±0.10	0.07	0.32	18.50±0.13	5.98±1.26	...
SMC	9	0.3±0.2	2.70±0.10	...	2.71±0.10	0.24	0.13	18.99±0.05	2.50±1.68	...
M33	6	4.6±0.9	6.27±0.03	4.11±0.04	2.87±0.10	0.33	0.18	24.64±0.09	4.27±0.89	12.6±2.7
		< 0.45							< 0.41	< 1.22
M101	6	12±4	8.31±0.09	5.51±0.05	3.24±0.11	0.05	0.04	29.34±0.10	1.01±0.35	1.63±0.57
M51	4	18±7	8.96±0.06	5.05±0.03	3.43±0.10	0.30	0.16	29.42±0.27	1.53±0.61	1.44±0.67
M100	4	25±12.5	10.05±0.08	6.59±0.04	3.84±0.20	0.10	0.11	31.04±0.09	1.12±0.57	1.90±0.97
M31	3	29±4	4.36±0.02	0.98±0.02	3.85±0.10	0.67	0.35	24.42±0.10	1.45±0.28	5.25±0.88
M81	2	24±8	7.89±0.03	3.83±0.02	3.99±0.10	0.34	0.35	27.80±0.08	1.64±0.56	2.73±0.94
NGC5128	-2	28±7	7.84±0.06	3.94±0.02	3.38±0.11	0.00	0.50	28.12±0.14	2.84±0.76	2.67±0.75
NGC1316	-2	135±45	9.42±0.08	5.59±0.02	4.15±0.20	0.00	0.09	31.66±0.17	1.61±0.55	2.33±0.86
M87	-4	91±34	9.59±0.04	5.81±0.02	4.17±0.10	0.00	0.10	31.03±0.16	2.20±0.83	3.43±1.38
VirgoEs	-4	160±57	9.46±0.10	...	4.26±0.11	0.00	0.09	31.17±0.09	2.79±1.03	...
M49	-5	100 ⁺³⁵ ₋₃₀	9.37±0.06	5.40±0.03	4.30±0.10	0.00	0.09	31.06±0.10	1.71±0.61	2.52±0.91

^aNova Rate References: LMC: Capaccioli et al. (1990). SMC: Graham (1979). M33: Della Valle et al. (1994) and Sharov (1993). M101, M51: Shafter et al. (2000). M100: Ferrarese et al. (1996). M31: Capaccioli et al. (1989). M81: Moses & Shafter (1993). NGC5128: Ciardullo et al. (1990). NGC1316: Della Valle & Gilmozzi (2002). M87: Shafter et al. (2000). Virgo: Pritchett & van den Bergh (1987). M49: this paper.

^bColor References: LMC, SMC, M33, M101, M51, M31, M81, NGC5128, M87, Virgo: Shafter et al. (2000). M100: Aaronson (1978). NGC1316: Della Valle (2002). M49: $(B - V)_0$ from NED and $(V - K)_0$ from Frogel et al. (1978).

^cErrors on the internal and Galactic extinction estimates are assumed to be 20% and 16% respectively (the latter from Schlegel et al. 1998).

^dDistance References: LMC, SMC, M33, M101, M31, M81, M100: Ferrarese et al. (2000). M51, NGC5128, NGC1316, M87, M49, Virgo: Tonry et al. (2001).